X-521-70-404
PREPRINT

PROPAGATION DELAY IN THE ATMOSPHERE

DAVID M. LeVINE

NOVEMBER 1970

GSFC

GODDARD SPACE FLIGHT CENTER
GREENBELT, MARYLAND

X-521-70-404

PROPAGATION DELAY IN THE ATMOSPHERE

David M. LeVine*
University of Maryland
College Park, Maryland

November 1970

GODDARD SPACE FLIGHT CENTER
Greenbelt, Maryland

*This work was done as part of the NASA-ASEE Summer Faculty Fellowship program (1970) and prepared for the Timing Systems Section of Advanced Development Division.

PROPAGATION DELAY IN THE ATMOSPHERE

David M. LeVine
University of Maryland

ABSTRACT

The structure of the lower atmosphere and the ionosphere are discussed and an introduction to ray tracing in the atmosphere is given. Models for each region appropriate for satellite-to-earth communication in the frequency range 1 GHz to 15 GHz are discussed. Assuming a spherically symmetric atmosphere, propagation delay is computed for the lower atmosphere and for the ionosphere. The total atmospheric delay is also computed as a function of atmospheric conditions, frequency and altitude of the signal source.

CONTENTS

PROPAGATION DELAY IN THE ATMOSPHERE

I. INTRODUCTION

The problem which motivated this investigation was an analysis of the limits which the atmosphere places on a one-way satellite-borne system for clock synchronization. Presumably an atomic clock is to be placed aboard a satellite to beam timing information to the ground. Ideally such a clock would be able to beam the timing information to stations which are widely distributed over the globe and which are equipped with only minimal receiving equipment. However, in such a one-way timing system, a correction for the finite velocity of propagation of the signal is necessary in order to obtain practical synchronization. For example, in vacuum, it would take about 3 milli-seconds for a signal to reach the ground from a satellite 1,000 km above the receiving station; however, present demand exists for micro-second synchronization and present state of the art is about one-tenth of a micro-second. An obvious first order correction to account for the propagation delay is to use the straight line distance between satellite and receiver (slant range) divided by the speed of light in vacuum. Presuming that the relative position of satellite and receiver is known with sufficient accuracy, this provides a simple correction easily implemented by the receiver. A major objective of this report is to provide sufficient information about propagation delay in the atmosphere to permit a quantitative evaluation of such a correction scheme.

This report is intended to be tutorial and to lay the basis for continued research as much as to be a vehicle to report on the author's work. Consequently, the first three sections of this report are devoted to background material consisting of a brief summary of the general structure of the atmosphere and the background for simple ray tracing. Emphasis is placed on available models of the atmosphere because they have been used in the past, and will continue to be used for predictions until an improved model, with easily determined parameters, is developed. The remainder of the report is devoted to the calculations made by the author. Calculations of time delay have been made using up-to-date models for a variety of atmospheric and geometric conditions. Data is presented for the propagation delay in the lower atmosphere, the ionosphere and for the composite atmosphere.

II. THE LOWER ATMOSPHERE

A. Introduction

The atmosphere can be separated into many regions. This is done most frequently on the basis of the temperature gradient of the atmosphere, on the basis of its composition, or on the basis of its electrical properties.

Between sea level and about 100 km the temperature profile of the atmosphere consists of alternate regions of increasing or decreasing temperature separated by regions of relatively constant temperature. For example, between the earth's surface and about 6 to 15 km, depending on the season and location, the average temperature decreases at about 6.5°K per kilometer. This region is referred to as the troposphere and is that region of the atmosphere which is directly associated with rain, clouds and those other phenomena generally called weather. Above the troposphere is a thin region of relatively constant temperature called the tropopause which is followed by a region of slowly increasing temperature called the stratosphere. The stratosphere is a region of generally laminar flow and is characterized by the relatively abundant presence of ozone, and it ends at about 50 km in another region of relatively constant temperature called the stratopause. Above the stratopause is the mesosphere, a region of high velocity turbulent winds, in which the temperature once again decreases up to about 80 km where it ends in another thin region of constant temperature called the mesopause. Above the mesopause lies a thick region of ill defined extent called the thermosphere in which the temperature increases. However, at the heights of the thermosphere the composition of the atmosphere is no longer uniform, ionization by solar radiation becomes significant and the mean free path increases significantly. Consequently, care must be exercised when referring to "temperature" in this region. See Figure 1 for a typical temperature profile for the atmosphere[1] and definition of the regions.

Compositionally, the atmosphere is relatively homogeneous below the mesopause (about 80 km) and this region is often referred to as the homosphere. The homosphere consists, by volume, of about 78.08 percent of molecular nitrogen, 20.94 percent of molecular oxygen, .93 percent argon and traces of such elements as helium, krypton, neon and xenon. The mean molecular weight in the homosphere is about 28.97. Another important constituent of the atmosphere is water vapor; However, its content is extremely variable although the amount of water vapor decreases rapidly with altitude and is almost negligible above the tropopause. Above the homosphere the elements of the atmosphere begin to separate by diffusion and the chemical composition is changed due to dissociation caused by solar radiation. This region is often called the heterosphere. In the heterosphere molecular oxygen becomes dissociated by solar radiation and rapidly becomes the dominant component of the atmosphere, but eventually the lighter

elements, helium and hydrogen (produced by dissociation of other atmospheric gases) diffuse upward and become dominant. In fact, evidence exists to suggest the existence of a region dominated by the presence of helium and lying somewhere between 1,000 and 2,000 km and given the name heliosphere. The region above the heliosphere is predominately composed of hydrogen. At heights of about 700 to 1,500 km the mean free path has increased sufficiently and kinetic energy of the constituents has increased sufficiently that a significant portion of the atmospheric gas can escape the earth's gravitational field. However, the atmosphere as such does not end here but rather merges gradually with the extended solar atmosphere. The region out to many earth radii but within the magnetosphere contains protons and electrons emitted from the sun and this region is sometimes called the protonosphere. It extends down to between 1,000 and 5,000 km.

In terms of its effect on wave propagation the atmosphere separates naturally into two regions which are distinguished by the occurrence of photoionization of the atmospheric gas. Above about 60 km the atmosphere is very sparse as compared to the surface and would for all practical purposes be negligible from a propagation point of view were it not for the fact that at this altitude a significant portion of the gas becomes ionized by solar radiation. The resultant plasma can have a great effect on wave propagation, and this region is called the ionosphere. The atmosphere below 60 km will be called the "lower atmosphere" and is distinguished from the ionosphere in that it is a relatively dense gas of neutral particles. The lower atmosphere contains practically all of the atmosphere, the density at 60 km being about 10^{-4} of its surface value.

B. The Electrical Properties of the Lower Atmosphere

The relative dielectric constant of a gas is given in terms of the polarizibility, α_0, of the individual molecules by the Clausius-Mossotti relationship:

$$\frac{\epsilon_r - 1}{\epsilon_r + 2} = \frac{N_0 \rho}{3M} \alpha_0 \qquad \text{II-1}$$

where ϵ_r is the relative dielectric constant, N_0 is Avogadro's number, M is the molecular weight and ρ is the density of the gas. If, in addition, the molecules have a residual dipole moment, m_0, the Clausius-Mossotti formula can be generalized to account for the alignment of those dipoles by the external field.

In this case:

$$\frac{\epsilon_r - 1}{\epsilon_r + 2} = \frac{N_0 \rho}{3M} \left\{ \alpha_0 + \frac{m_0^2}{3\epsilon_0 kT} \frac{1}{(1 - j\omega\tau)} \right\} \qquad \text{II-2}$$

where ω is the frequency of the external field and τ is the relaxation time. For frequencies less than about 100 GHz the term $\omega\tau$ is negligible for air.[2, 3] Neglecting the loss term and assuming that air behaves like an ideal gas (i.e., ρ is proportional to the ratio of pressure to temperature) and that $\epsilon_r \simeq 1$, one finds that:

$$\epsilon_r - 1 = \sum_{i=1}^{N} K_i \frac{P_i}{T} + \sum_{j=1}^{N'} \frac{P_j}{T} \left[A_j + \frac{B_j}{T} \right] \qquad \text{II-3}$$

where P_i is the partial pressure of each non-polar component of air and P_j is the partial pressure of the components with polar molecules. (The only significant component with polar molecules is water vapor and the important non-polar components are "dry air" and CO_2. The K_j, A_j and B_j are constants and T is the temperature.

Equation II-3 can be solved for the index of refraction, $\eta = \sqrt{\mu_r \epsilon_r}$, and for air the approximation $\mu_r = 1$, $\epsilon_r - 1 \ll 1$ are good. Hence $\eta = \sqrt{\epsilon_r} \simeq 1 + (1/2)\left(\epsilon_r - 1\right)$ is a good approximation for air. However, rather than use the index of refraction directly it proves convenient to define a new quantity, the refractivity, N, by the relationship: $N = (\eta - 1) \times 10^6$. Then, it follows from Equation II-3 that:

$$N = A \frac{P}{T} + B \frac{P_w}{T} + C \frac{P_w}{T^2} \qquad \text{II-4}$$

The constants A, B and C depend on the molecular properties of the atmospheric gases — on their polarizability and permanent dipole moment — and are obtained by measurements of the atmospheric gas. P is the total pressure of air and P_w is the partial pressure of water vapor. The most frequently used values for the constants are due to Smith and Weintraub.[4] Using their values:

$$N = 77.6 \frac{P}{T} - 6 \frac{P_w}{T} + 3.75 \times 10^{+5} \frac{P_w}{T^2} \qquad \text{II-5}$$

where T is measured in °K and pressure is measured in millibars. This formula is accurate to within 1/2 percent; however, it is usually approximated with small error by:

$$N = \frac{77.6}{T}\left[P + \frac{4810}{T} P_w\right] \qquad \text{II-6}$$

Note that Equation II-6 is frequency independent. The lower atmosphere appears to be independent of frequency below about 30 GHz[3] when dispersive effects due to water vapor and oxygen absorption lines become important.

C. Models for the Lower Atmosphere

Ideally one can obtain the information about refractivity for propagation studies from Equation II-6 and measured values of T, P and P_w. Unfortunately, for purposes of satellite communications, knowledge of these parameters is required over a very great range of vertical and horizontal distances, over which simultaneous measurement of these parameters is difficult. One alternative approach is to build an idealized model of the atmosphere starting, for example, with the assumption that the atmosphere is an ideal, stationary gas and using a realistic model for its temperature profile and the gravitational field. With some mean parameters such as surface density and composition as boundary conditions, this model could be used to construct, analytically, profiles for other atmospheric parameters. This data could be used in II-6 to obtain an "ideal" model of refractivity as a function of altitude. One such model is the U.S. Standard Atmosphere, 1962.[5] Unfortunately, this is not a very satisfactory method because even the average diurnal and seasonal changes in atmospheric properties are not represented. A somewhat more feasible approach is to observe N(h) at many locations over long periods of time and then construct models for the refractivity based on the long-term mean values, perhaps with a parameter or two with which to tie the model to geographical and temporal changes in the mean properties. A number of such models exist.

The earliest of these models were based on the following general characteristics of the refractivity:[6, 7, 8]

1. The refractivity varies between about 200 and 450 with 313 being the mean value for the continental U. S.

2. Between the surface and 1 km, the refractivity is roughly a linear, decreasing function of altitude.

3. There is a strong correlation between the mean surface value of refractivity, N_s, and the change in N between the surface and 1 km: $-\Delta N = \alpha e^{\beta N_s}$ where $\alpha = 7.32$ and $\beta = .005577$ for the U. S.

4. The value of N at 9 km above sea level is extraordinarily constant at about 105.

Among the models for the refractivity which are based on these properties are the following:

a. Linear Model: In this model $N(h) = N_s + \Delta N(h - h_s)$ where h is the height above sea level and h_s is the height of the surface above sea level, both measured in kilometers. A linear function of altitude permits use of an "effective earth's radius" model to facilitate ray tracing, and is a good approximation close to the earth's surface. It is useful for line-of-sight communications between earth-bound stations but is not accurate enough at high altitudes to be used in satellite-to-earth propagation delay studies.

b. The CRPL Reference Atmosphere (1958) Model: This model has three parts:

$$N(h) = N_s + \Delta N(h - h_s) \qquad h_s \leq h < h_s + 1$$

$$= (N_s + \Delta N)\, e^{-a[h-h_s-1]} \qquad h_s + 1 \leq h < 9$$

$$= 105\, e^{-b[h-9]} \qquad h \geq 9 \qquad \text{II-7}$$

where $a = [1/(8 - h_s)]\, \ln[(N_s + \Delta N)/105]$ and $b = .1424$. This model has the advantages of allowing an "effective earth's radius" approach for low altitude uses and of providing a good match to the data for higher altitudes. Its coefficients have been chosen from a least squares match to the Rocket Panel data.[6, 9]

c. The CRPL Exponential Reference Model: In this case N(h) is approximated by a single exponential:

$$N(h) = N_s\, e^{-C_e(h-h_s)} \qquad \text{II-8}$$

where

$$C_e = \ell n \frac{N_s}{N_s + \Delta N} \qquad \text{II-9}$$

This model has the advantages of relative simplicity and continuity of dN/dh. However, it is tied to the low altitude values of refractivity (i.e. N_s and ΔN) and is not as accurate a representation of N(h) at higher altitudes as is the CRPL Reference Atmosphere.(6, 8)

Each of the preceding models really depend on only one parameter, the surface value of refractivity, N_s, because the relationship $\Delta N = -\alpha e^{\beta N_s}$ is used either explicitly or implicitly. This was done intentionally to tie the models as simply as possible to the local atmospheric conditions. For example, such models could be used to correct for atmospheric effects on propagation at receiving stations equipped with only the minimal amount of meterological equipment needed to measure N_s and, particularly, without detailed monitoring of the upper atmosphere. On the other hand, the availability of only one parameter limits the accuracy with which the models can be made to fit the mean refractivity profiles.

d. The Bi-Exponential Model: The index of refraction depends explicitly on the partial pressure of water vapor, yet none of the preceding models explicitly take this dependence into account. The bi-exponential model does so while, at the same time, increasing the number of parameters available for curve fitting. This model consists of one exponential for the "dry-term" in Equation II-6 and one for the "wet-term." Thus:

$$N(h) = De^{-(h-h_s)/H_d} + We^{-(h-h_s)/H_w} \qquad \text{II-10}$$

where D is the refractivity of dry air at the earth's surface, W is the refractivity due to water vapor at the earth's surface, H_d is the scale height of dry air and H_w is the scale height of water vapor.

There is some theoretical justification for this model because assuming that the lower atmosphere can be approximated by an ideal gas in a uniform gravitational field, one finds that at constant temperature the pressure varies exponentially with altitude. In such an atmosphere, Equation II-6 has the form of the bi-exponential model. A difficulty with the model is that the two scale heights, H_d

and H_w, are not easily obtained: D and W can be obtained by on-site measurements of pressure, temperature and humidity, but H_d and H_w can only be obtained by curve fitting to detailed measurements of N(h). On the other hand, maps of average values of the scale heights can be prepared.[8] Of course, the value of such a system depends on their diurnal and seasonal variability. Typically $8.0 \leq H_d \leq 11$ and $1.5 \leq H_w \leq 4.0$ for the U. S.[8] Both are generally higher in summer than in winter. $D = 77.6\left(P_d/T\right)$ and $W = 3.73 \times 10^5\left(P_w/T^2\right)$ [RH/100] where RH is the relativity humidity in percent. (It is to be noted that some discussion exists as to the global validity of the bi-exponential model.[10, 11])

e. The Compound Bi-Exponential Model: This is among the latest and perhaps the most representative in the sequence of models for the refractivity. The lower atmosphere consists of two temperature regimes: the troposphere and the stratosphere. The compound bi-exponential model, by adding two additional parameters to the bi-exponential model, attempts to take the different atmospheric properties of these two regions into account while at the same time keeping the virtues of a separate treatment for wet and dry terms. Thus, the compound bi-exponential model consists of:

$$N(h) = De^{-(h-h_s)/H_{d_1}} + We^{-(h-h_s)/H_w} \qquad h_s \leq h < h_t$$

$$= De^{-\left[\left(h_t-h_s\right)/H_{d_1} + \left(h-h_t\right)/H_{d_2}\right]} + We^{-(h-h_s)/H_w} \qquad h \geq h_t \quad \text{II-11}$$

where D, W and H_w are as defined for the bi-exponential model and H_{d_1} is the scale height for the troposphere, H_{d_2} is the scale height above the troposphere, and h_t is the height above sea level of the bottom of the tropopause (top of the troposphere).

The scale heights and h_t must be determined from available data, for example, by making a least squares fit; consequently, this model is strictly applicable only where complete data is available. However, compilation of refractivity profiles over a five year period have been achieved at a number of stations and the 5-year means used to obtain world wide maps of the various parameters required for use of the compound bi-exponential model.[12]

Because it incorporates more of the physical structure of the atmosphere and because it has more parameters, the compound bi-exponential model is the most representative of available models. It represents, usually to within one or two units of refractivity (standard deviation), the observed mean profiles, N(h). The

representation is often better than this; however, there are a number of regions on the globe where the representation is much worse. These lie within a strip ±30° latitude on either side of the equator, predominately over the seas and over India.(12)

III. THE IONOSPHERE

A. Introduction

Compared to the lower atmosphere the ionosphere is a region of relatively low density and heterogeneous composition. The maximum density in the ionosphere is about 10^{-7} g/cc and at 400 km less than 10^{-14} g/cc; whereas, the density of the earth's atmosphere at sea level is about 10^{-3} g/cc. In addition, beginning very near the bottom of the ionosphere the atmospheric gas is no longer kept homogeneous by turbulent mixing but begins to separate by diffusion into layers of the constituents. The percentage of nitrogen decreases and that of oxygen increases. Near the top of the ionosphere the presence of helium becomes important, forming a layer between about 1,000 and 2,000 km; and beyond the heliosphere hydrogen is the predominate element.

The charged particles in the ionosphere are primarily the result of ionization by the short wavelength (less than 2,000 Å) end of the solar spectrum. The major contributors are singly ionized atomic and molecular nitrogen and oxygen and nitric oxide. However, especially near the top of the ionosphere, the concentration of ions and electrons is appreciably affected by the influx of particles from the sun.

Early investigators of the ionosphere thought that it was composed of layers and the names D, E and F apparently applied by Appelton[13] came into wide use. However, what was originally mistaken for layers were in reality relative peaks in the electron density profile. Even so, the ionosphere is still separated into a number of regions or layers associated with these peaks. They are:

1. The D-Region: The D-region is the lowest-most region of the ionosphere, extending roughly from 60 to 90 km. Surprisingly enough it is a region about which relatively little is known because of the difficulty of making measurements. Typical electron densities vary from abcut 10 - 100 electrons/cc at 70 km to 10^3 - 10^5 electrons/cc at 90 km. Occasionally large increases in D-region ionization occur which apparently correlate with different types of solar disturbances.[14] The D-region is the ionospheric region of highest attenuation, and the primary sources of ionizing radiation appear to be Lyman-α (1216 Å), cosmic rays and some x-rays (2 - 8 Å).[15]

2. The E-Region: The E-region lies just above the D-region, from about 90 km to between 120 to 140 km, with the peak density generally occurring at about 110 km. The E-region was the first ionospheric region to be observed (by Appelton and Barnett, 1925) and has been extensively studied since then. It is an unusually regular region for the ionosphere although there appear to be irregular increases in electron density within the E-region whose origins are not

well understood. These phenomena are referred to as sporadic-E and the otherwise well behaved region is called the normal E-region or just the E-region.

The normal E-region apparently responds to the soft X-ray portion of the solar spectrum (10 - 170 Å) and to Lyman-β (1026 Å) which ionize O_2.[15] Electron loss is by recombination, and a Chapman layer[16, 17] with recombination loss is a good approximation to the normal E-region. The peak electron density of the E-region is about 10^5 electrons/cc with 50-60% variation with solar activity, and to a good first approximation the maximum electron density is given by:[18, 14]

$$N_M = 10^4 \sqrt{(180 + 1.44R)\cos\chi} \qquad \text{III-1}$$

where R is the mean Zurich sunspot number and χ is the solar zenith angle. At night the electron density decreases sufficiently to make the E-region difficult to observe. The geographical variations in the morphology of the E-region are slight.

3. The F-Region: The F-region is the ionospheric region of greatest electron density. It extends from the top of the E-region to between 700 and 1500 km, and it is frequently sub-divided into two regions: F_1 and F_2.

The F_1 region is located at the bottom of the F-region near the E-region. Its peak electron density generally occurs near 160 km and it has a half-thickness of about 50 km. The F_1 region is generally well defined only in the summer during the day. When it is evident, it behaves very much like a Chapman layer with electron loss via recombination; however, there are many seasonal and geographical anomalies. The peak electron density is given to a first approximation by:[18]

$$N_M = 1.24 \times 10^4 [4.3 + .01R]^2 \cos^{4/10}\chi \qquad \text{III-2}$$

Ionized molecular oxygen appears to be the major contributor to the F_1-region.

The F_2-region is a region of large electron density and large variations. A peak density of 2.5×10^5 electrons/cc at a height of about 250 km appears to be characteristic of the quiet F_2-region, and under quiet conditions the F_2-region is largely represented by a recombination Chapman layer.[19] However, the

F_2-region is a region of great variability and is strongly tied to the geomagnetic field. In addition, it is affected by tides and is apparently subject to strong internal electrical forces. Strong fluctuations in F_2 are more often associated with "magnetic storms" than electromagnetic outpourings of the sun, and the peak electron density may be as high as 10^7 electrons/cc. Among the anomalous behaviour of the F_2-region is the occurrence at middle latitudes of larger electron density in the winter than in the summer. In addition, the phenomena of spread-F appears to indicate a dynamic, turbulent F_2-region. In light of its many variations and anomalies, analytic prediction of the morphology of F_2 seems impossible at present and mapping the only feasible approach.

4. The Upper Ionosphere: The upper extremities of the F-region correspond to an atmospheric region of decreasing density and increasing temperature and mean free path. If the earth were in vacuum, particles would eventually escape the earth's gravitational field and the atmosphere would eventually decay to zero. However, the earth is imbedded in a continual stream of particulate radiation which emanates from the sun and which manifests itself near the earth in the form of a nearly fully ionized plasma of protons and electrons, often called the protonosphere.

The electron content of the ionosphere above the F_2 peak has been measured only relatively recently. Indications are that the density at 1,000 km above the earth's surface depends on the magnetic dip angle, m, and the zenith angle of the sun and is given to a first approximation by:[20]

$$N_e\,(1000\,\text{km}) = 8 \times 10^3 \left[1 + \cos^2 m \cos^2 \frac{\chi}{2}\right] \qquad \text{III-3}$$

Incoherent scatter measurements indicate that the density of electrons at 5,000 km is of the order of 10^3 electrons/cc.[20]

Typical density profiles for the ionosphere are shown in Figure 2.

B. Model for the Ionosphere

A plasma is a difficult many bodied problem because of the electrical interactions between particles. Alternate approaches to the plasma are equations for its distribution function or equations for the moments of the distribution function. Either approach is in general overwhelmingly difficult. However, in the special case of a zero temperature plasma and with losses proportional to the current density, the distribution function in velocity space becomes unusually amenable to analysis. In the case of an harmonic excitation whose frequency is

great enough to neglect the motion of the relatively massive ions in comparison to the electrons, one can represent the plasma by an effective conductivity tensor, $\overline{\sigma}$:

$$\overline{\sigma} = -\frac{j\omega_p^2 \epsilon_0}{Q\left[Q^2 - \omega_c^2\right]} \begin{bmatrix} \omega_{cx}^2 - Q^2 & -\left(jQ\omega_{cz} + \omega_{cx}\omega_{cy}\right) & \left(\omega_{cz}\omega_{cx} - jQ\omega_{cy}\right) \\ \left(jQ\omega_{cz} - \omega_{cx}\omega_{cy}\right) & \omega_{cy}^2 - Q^2 & -\left(\omega_{cz}\omega_{cy} + jQ\omega_{cx}\right) \\ \left(\omega_{cx}\omega_{cz} + jQ\omega_{cy}\right) & \left(jQ\omega_{cx} - \omega_{cz}\omega_{cy}\right) & \omega_{cz}^2 - Q^2 \end{bmatrix} \quad \text{III-4}$$

where $Q = \omega(1 + jZ)$, $Z = \nu_c/\omega$, ν_c is the collision frequency (the loss term is approximated by $-\nu_c \bar{J}$ where $\bar{J}$ is the current density), $\omega_p = \sqrt{q^2 N/M\epsilon_0}$ is the plasma frequency, $\omega_c = |q|B/M$ is the cyclotron frequency, $\omega_{ci} = |q|\left(\bar{B} \cdot \hat{a}_i\right)/M$ where $i = x, y$ or z, and N is the electron density.

The expression for the conductivity can be substituted into Maxwell's equations to obtain a description for the electromagnetic fields. The resultant equations happen to be equivalent to those obtained for a medium with tensor dielectric constant $\overline{\epsilon} = \epsilon_0 \overline{\epsilon}_r = \epsilon_0 \left[1 + j\left(\overline{\sigma}/\omega\epsilon_0\right)\right]$.

The index of refraction, η, for the hypothetical dielectric medium is obtained in a straight forward manner by seeking solutions to Maxwell's equations in the form of plane waves: $\bar{E} = E_0 e^{j(\bar{k}\cdot\bar{x} - wt)}$ where $\bar{k} \cdot \bar{k} = k_0^2 \eta^2$. In the case that the wave propagates in the z-direction one finds:

$$\eta^2 = 1 - \frac{X}{(1 - jZ) - \frac{Y_T^2}{2(1 - X - jZ)} \pm \sqrt{\frac{Y_T^2}{4(1 - X - jZ)^2} + Y_L^2}} \quad \text{III-5}$$

where $X = \left(\omega_p/\omega\right)^2$, $Y_L = \left(\omega_c/\omega\right)\cos\theta$, $Y_T = \left(\omega_c/\omega\right)\sin\theta$, and θ is the angle between the earth's magnetic field and the z-axis.[21] This relationship is attributed to Appelton and Hartree and is referred to as the Appelton-Hartree dispersion equation. It is the result of neglecting all thermal motion of the plasma particles and although useful in most radio communication problems cannot be used when plasma modes are important.

For ionospheric plasmas the maximum plasma frequency is about 20 MHz and the maximum cyclotron frequency is about 2 MHz. The collision frequency is greatest in the D-region of the ionosphere, decreasing to about 5×10^6 at the bottom of the E-region.[13] In the F_2-region the collision frequency is generally less than 3×10^3 collisions per second. Consequently, at frequencies in excess of a few hundred MHz, the ionosphere is essentially lossless, and the index of refraction is given by:

$$\eta^2 = 1 - \frac{X}{1 - \frac{Y_T^2}{2(1-X)} \pm \sqrt{\frac{Y_T^2}{4(1-X^2)} + Y_L^2}} \qquad \text{III-6}$$

The two solutions of this equation are called ordinary (+) and extraordinary (-) modes.

In the special case of propagation along the earth's magnetic field ($\theta = 0$), and neglecting loss, one obtains:

$$\eta^2 = 1 - \frac{X}{1 \pm Y^2} \qquad \text{III-7}$$

Checking the polarization of the waves corresponding to each solution indicates that both the ordinary and extraordinary waves are circularly polarized but in opposite senses. Since the two waves propagate at different velocities, an incident plane polarized wave undergoes a change in the direction of polarization (Faraday rotation) in traversing the plasma.

For frequencies above a few hundred MHz, the distinction between ordinary and extraordinary modes becomes quite small and is insignificant for frequencies above about 1,000 MHz.[22] In this case:

$$\eta^2 = 1 - \left(\frac{\omega_p}{\omega}\right)^2 \qquad \text{III-8}$$

Thus, at frequencies in the GHz and higher region, the plasma is essentially an isotropic, dispersive dielectric. The index of refraction varies as the square of the electron density.

No satisfactory model for the electron density in the ionosphere which predicts the diurnal, seasonal and geomagnetic variations in the density is presently available. This is a reflection of the complexity of the problem: The ionosphere is a dynamic region which depends on both the electromagnetic and particulate solar radiation, on the tides and on internal electrical forces. However, the primordial force in the ionosphere appears to be photoionization by radiation in the short wavelength end of the solar spectrum, and for this there is a good model which can be used as a starting point.

Chapman studied photoionization in the atmosphere even before the ionosphere was observed. In fact, on the basis of his studies he predicted an ionosphere. Assuming a monochromatic source of radiation, a homogeneous atmosphere composed of an ideal gas with molecules of mass, M, at temperature, T, and in a uniform gravitational field with gravitational constant g, Chapman showed that the rate of photoionization in a planar earth was:(16, 17)

$$q(\chi, z) = q_0 e^{[1 - z - \sec \chi e^{-z}]} \qquad \text{III-9}$$

where q_0 is the maximum rate of ion production, $z = (h - h_m)/H$, h is the altitude, h_m is the height of maximum rate, $H = kT/Mg$ and χ is the solar zenith angle. Assuming a process of electron loss such as recombination or attachment, and that equilibrium is reached between loss and generation, one can relate $q(\chi, z)$ to electron density. For recombination loss one obtains:

$$N(\chi, z) = N_0 \exp\left\{\frac{1 - z - \sec \chi e^{-z}}{2}\right\} \qquad \text{III-10}$$

and for attachment loss:

$$N(\chi, z) = N_0 \exp\left\{1 - z - \sec \chi e^{-z}\right\} \qquad \text{III-11}$$

where N_0 is the maximum electron density.

That the Chapman analysis is essentially correct is reflected in the strong resemblence of many of the ionospheric regions (especially in the quiet ionosphere) to a Chapman layer. This is especially so in the lower ionosphere, particularly in the normal E-region. To a first approximation, the ionosphere is composed of a series of Chapman layers roughly corresponding to each of the ionospheric regions. On the other hand, there are very many anomalies in a Chapman model for the ionosphere, which reflects the complex set of ingredients which comprise the ionosphere.

One approach to modeling the electron density profile is to attempt to match a number of Chapman functions to observed data, perhaps with some help from the rule-of-thumb formulae for peak densities presented in the previous section. An additional exponential function is generally required for the upper regions of the ionosphere. However, the Chapman functions are rather awkward to deal with, and since the data and fit are likely to be rather approximate anyway, some simplifying assumptions can be made. A realistic approach[22] is to use parabolas to model the peak density due to D, E, F_1, and the bottom of F_2-regions (the Chapman function is approximately a parabola near $z = 0$). The top of the ionosphere between the peak of the F_2-region and about 1,000 km often is Chapman-like varying as $\exp\frac{1}{2}\left[1 - h - e^{-h}\right]$ and can be so modeled; an exponential can be used for the upper ionosphere.

IV. RAY TRACING

A. Geometrical Optics

Consider a medium whose dielectric properties are slowly varying functions of position. Since Maxwell's equations admit solutions in the form of plane waves when ϵ and μ are constants, it seems reasonable to attempt a solution in the case of slowly varying dielectric properties with functions which resemble plane waves. Thus guess solutions in the form:

$$\bar{E}(\bar{r}, t) = \bar{\mathcal{E}}(\bar{r})\, e^{j(kS(\bar{r})-\omega t)} \qquad \text{IV-1a}$$

$$\bar{H}(\bar{r}, t) = \bar{\mathcal{H}}(\bar{r})\, e^{j(kS(\bar{r})-\omega t)} \qquad \text{IV-1b}$$

where $k = \omega/\epsilon$, $c = 1/\sqrt{\mu\epsilon}$. Substituting Equations IV-1 into Maxwell's equations for sourceless dielectrics, one obtains:

$$\nabla S \times \bar{\mathcal{E}} - \mu c\, \bar{\mathcal{H}} = j\frac{1}{k}\nabla \times \bar{\mathcal{E}} \qquad \text{IV-2a}$$

$$\nabla S \times \bar{\mathcal{H}} + \epsilon c\, \bar{\mathcal{E}} = j\frac{1}{k}\nabla \times \bar{\mathcal{H}} \qquad \text{IV-2b}$$

$$\bar{\mathcal{E}} \cdot \nabla S = j\frac{1}{k}\left[\bar{\mathcal{E}} \cdot \nabla \ln \epsilon + \bar{\nabla} \cdot \bar{\mathcal{E}}\right] \qquad \text{IV-2c}$$

$$\bar{\mathcal{H}} \cdot \nabla S = j\frac{1}{k}\left[\bar{\mathcal{H}} \cdot \nabla \ln \mu + \bar{\nabla} \cdot \bar{\mathcal{H}}\right] \qquad \text{IV-2d}$$

Introducing the variables $\tilde{\chi}_i = kx_i$ and the new quantities $\bar{e} = \epsilon_0 \bar{\mathcal{E}}$, $\bar{h} = \mu_0 \bar{\mathcal{H}}$, $\tilde{S} = kS$, one obtains:

$$\tilde{\nabla}\tilde{S} \times \bar{e} - \mu_r \bar{h} = j\tilde{\nabla} \times \bar{e} \qquad \text{IV-3a}$$

$$\tilde{\nabla}\tilde{S} \times \bar{h} + \epsilon_r \bar{e} = j\tilde{\nabla} \times \bar{h} \qquad \text{IV-3b}$$

$$\bar{e} \cdot \tilde{\nabla S} = j\left[\bar{e} \cdot \nabla \ell n \epsilon_r + \nabla \cdot \bar{e}\right] \qquad \text{IV-3c}$$

$$\bar{h} \cdot \tilde{\nabla S} = j\left[\bar{h} \cdot \nabla \ell n \mu_r + \nabla \cdot \bar{h}\right] \qquad \text{IV-3d}$$

where the operator $\tilde{\nabla} = k\nabla$ and $\bar{e}$ and $\bar{h}$ have the same dimensions. μ_r and ϵ_r are dimensionless.

Consequently, if the change in $\bar{e}$ and $\bar{h}$ are small in one (free space) wavelength, then approximately:

$$\tilde{\nabla S} \times \bar{e} - \mu_r \bar{h} = 0 \qquad \text{IV-4a}$$

$$\tilde{\nabla S} \times \bar{h} + \epsilon_r \bar{e} = 0 \qquad \text{IV-4b}$$

$$\bar{e} \cdot \tilde{\nabla S} = 0 \qquad \text{IV-4c}$$

$$\bar{h} \cdot \tilde{\nabla S} = 0 \qquad \text{IV-4d}$$

These equations describe a limiting case referred to as "geometrical optics".

Solving Equations IV-4 for $\tilde{\nabla S}$, yields:

$$(\tilde{\nabla S})^2 = (\nabla S)^2 = \eta^2 \qquad \text{IV-5}$$

This equation is referred to as the equation for the eikonal and its solution, $S(\bar{r})$, represents a collection of surfaces of constant phase. The locus of a unit vector perpendicular to these surfaces is called a ray. It is easily shown that for an isotropic, lossless medium, the time average Poynting vector is perpendicular to the surfaces of constant phase. Consequently, to the extent that the local Poynting vector represents the direction of energy flow, the tangent to a ray points in the direction of energy flow.

A useful differential equation for the rays follows from their definition.(23) Let s be the length of arc measured along the ray path and $\bar{r}(s)$ be the position

vector to a point on the ray. Then $d\bar{r}/ds$ is a unit vector tangent to the ray at s, and from the definition of a ray:

$$\frac{\nabla S(\bar{r})}{|\nabla S(\bar{r})|} = \frac{\nabla S(\bar{r})}{\eta} = \frac{d\bar{r}}{ds} \qquad \text{IV-6}$$

Therefore:

$$\eta \frac{d\bar{r}}{ds} = \nabla S(\bar{r}) \qquad \text{IV-7}$$

Differentiating both sides with respect to s one obtains the following vector differential equation for the ray, $\bar{r}(s)$:

$$\frac{d}{ds}\left[\eta \frac{d\bar{r}}{ds}\right] = \frac{d}{ds} \nabla S(\bar{r}) = \nabla \eta \qquad \text{IV-8}$$

The velocity with which a signal travels along a ray — i.e. the velocity with which the surfaces of constant phase expand in space — can be found by differentiating the equation for constant phase with respect to time. That is:

$$\frac{d}{dt}\left[kS(\bar{r}) - \omega t\right] = 0 \qquad \text{IV-9}$$

Using $(d/dt)\, S(\bar{r}) = \nabla S \cdot (d\bar{r}/dt)$ and $|\nabla S(\bar{r})| = \eta$ one obtains:

$$\frac{\nabla S}{|\nabla S|} \cdot \frac{d\bar{r}}{dt} = \frac{c}{\eta} = v_p \qquad \text{IV-10}$$

where v_p is the component of "phase velocity" along a ray.

If the medium is dispersive, the velocity of propagation of a signal loses precise meaning because the signal changes as it propagates. However, if the signal does not change too much, it can often be represented by a (spreading) envelope

which propagates at velocity:

$$v_g = \frac{1}{\left| \nabla \left(\frac{\partial}{\partial \omega} kS(\bar{r}) \right)_{\omega_0} \right|} \qquad \text{IV-11}$$

where ω_0 is the "center frequency" of the spectrum of the signal. v_g is called the group velocity.[25] In the special case of one dimension, one obtains:

$$v_g = \left. \frac{c}{\eta(\omega) + \omega \frac{\partial}{\partial \omega} \eta(\omega)} \right|_{\omega=\omega_0} \qquad \text{IV-12}$$

Equation IV-12 should also be a reasonable approximation for slowly varying media in which the solutions are locally well approximated by plane waves.

B. The Applicability of Geometrical Optics to the Atmosphere

The crucial assumptions underlying the development of geometrical optics are: 1) That the dielectric properties of the medium vary only slightly in one wavelength and 2) That the amplitude of the signal does not change significantly in one wavelength.

The latter assumption requires the exclusion of regions where many rays cross, such as at focal points, and the exclusion of regions in which diffraction is important, such as near the edges of a shadow. Neither of these regions occur in the spherically symmetric, slowly varying atmospheres considered in this report. The model atmospheres considered have no discontinuities in index of refraction. Also, in order that amplitude changes be small, regions of large attenuation must be neglected. However, at the frequencies considered here (1 to 15 GHz), attenuation per wavelength in the atmosphere is small;[24] In fact, all models of the atmosphere considered in this report are lossless.

The scale of variation of the atmospheric properties is a more complex question because both regions of the atmosphere have, in addition to gross features whose scale of variations is kilometers, local variations whose scale can be quite small. For example, the average index of refraction in the lower atmosphere is reasonably well modeled by the compound bi-exponential model whose scale heights

are of the order of kilometers. But this model describes only the gross features of the lower atmosphere and is based on information which smooths out any local fluctuations due to rain, clouds or turbulence. Similarly, gross features of the ionosphere are to a crude first approximation represented by a number of parabolas whose half-widths* are of the order of many kilometers. But on a small scale the ionosphere is a turbulent, inhomogeneous region, as such phenomena as spread-F make evident.

The local fluctuations in either atmospheric region are difficult to model and are complex phenomena whose effect on propagation is currently an active area of investigation. Consequently, it seems reasonable, especially in a first approach to the problem, to neglect the local fluctuations and treat only the gross features of the atmosphere. This is done here in the hopes that a discussion of the effects of local fluctuations will be the subject of further work.

C. Equations for the Time Delay

The time required for a signal to propagate between two points, p_1 and p_2 is given by:

$$\Delta t = \int_{p_1}^{p_2} \frac{1}{v}\, ds \qquad \text{IV-13}$$

where v is the appropriate signal velocity and the integration is taken along the ray path. The lower atmosphere is non-dispersive in the frequency regime of interest, so that v is the phase velocity. On the other hand, the ionosphere is dispersive and for frequencies above about one GHz, where the effect of the earth's magnetic field may be neglected, one has to a good first approximation, $\eta = \sqrt{1 - \left(\omega_p/\omega\right)^2}$. In this case, the group velocity is $v_g = c\eta$.

In order to determine the ray path, the assumption is made that the atmosphere is spherically symmetric. This first approximation means that horizontal inhomogeneities in the lower atmosphere such as accompany weather fronts and horizontal inhomogeneities in the ionosphere such as are the result of the geomagnetic dependence of the F_2-region and changes in the local solar zenith angle, will be neglected. This assumption has been made to permit a tractable solution to the problem of time delay. It should be a reasonable first approximation, especially if the maximum lateral dimension of the atmosphere through which propagation takes place is small compared to the scale of horizontal inhomogeneities.

*Half the distance between the intercepts on the axis corresponding to zero electron density.

In the case of a spherically symmetric atmosphere, it is easily shown that the vector $\bar{r} \times \eta(\bar{r})\bar{s}$ is constant along the ray. ($\bar{s}$ is a unit vector tangent to the ray at s.) Consequently, the rays lie in planes through the origin and $\eta(\bar{r})r \sin\phi$ is equal to a constant along the ray, where ϕ is the angle between $\bar{r}$ and $\bar{s}$. This relationship is sometimes called Bourguer's rule.

From Figure 3 it is apparent that $\sin\phi = r\,d\theta/ds = r\left[r^2 + (dr/d\theta)^2\right]^{-1/2}$. Consequently, $A/r\eta(r) = \sin\phi = r\left[r^2 + (dr/d\theta)^2\right]^{-1/2}$ where A is the constant in Bourguer's formula. Solving for $dr/d\theta$, one obtains:

$$\frac{dr}{d\theta} = \frac{r}{A}\sqrt{r^2\eta^2(r) - A^2} \qquad \text{IV-14}$$

Thus;

$$ds = \sqrt{1 + r^2\left(\frac{d\theta}{dr}\right)^2}\,dr = \frac{r\eta(r)}{\sqrt{r^2\eta^2(r) - A^2}}\,dr \qquad \text{IV-15}$$

The unknown constant A can be expressed in terms of the initial point (r_1, θ_1) and the final point (r_2, θ_2) of the ray by:

$$\theta_2 - \theta_1 = \int_{r_1}^{r_2} \frac{A\,dr}{r\sqrt{r^2\eta^2(r) - A^2}} \qquad \text{IV-16}$$

Expressions for the time required for a ray to travel a given path can now be obtained in the form of two coupled integral equations. In the case of the lower atmosphere, using the phase velocity, one obtains:

$$\Delta t = \frac{1}{c}\int_{p_1}^{p_2} \eta\,ds = \frac{1}{c}\int_{r_1}^{r_2} \frac{r\eta^2(r)\,dr}{\sqrt{r^2\eta^2(r) - A^2}} \qquad \text{IV-17}$$

where A is found from Equation IV-16. In the case of ionosphere, neglecting the effect of the geomagnetic field and losses, one obtains:

$$\Delta t = \frac{1}{c}\int_{p_1}^{p_2}\frac{ds}{\eta} = \frac{1}{c}\int_{r_1}^{r_2}\frac{r\,dr}{\sqrt{r^2\,\eta^2(r) - A^2}} \qquad \text{IV-18}$$

where $\eta = \sqrt{1 - \left(\omega_p/\omega\right)^2}$ and A is found from Equation IV-16.

The preceding two pair of equations have been solved for a number of combinations of $\eta(r)$ and geometry and the results are reported in the following section.

V. RESULTS

A. The Lower Atmosphere

The compound bi-exponential model was used to compute the time required for propagation in the lower atmosphere. The signal was assumed to start at various distances above the earth's surface ranging from an altitude of 50 km to 100 km, and for each altitude the time required for the signal to propagate to the earth was computed for many different paths. For each path, the actual aspect angle and the difference between the actual time required for propagation and the time which would be required in the absence of an atmosphere (free space path) were computed. The actual aspect angle is the angle which the straight line between sender and receiver makes with the vertical, measured at the receiving station. The difference between actual propagation delay and the free space propagation delay, which will be referred to henceforth as the "corrected time delay", is a significant characteristic of the path in two important respects: 1) It is an indication of the effect of the medium on propagation; 2) It is an indication of the efficacy of a simple first order correction to account for propagation delay in timing systems. (In order to obtain micro-second time accuracy in a one-way timing system, some correction for the propagation delay is necessary. A simple first order correction is to assume that the signal propagates along the straight line between sender and receiver at the speed of light in vacuum — i.e. neglect the medium. The corrected time delay is the error incurred in such a correction scheme.)

The compound bi-exponential model was used to describe the lower atmosphere because it is the latest and most detailed model of the lower atmosphere generally available at present. It is based on the five-year mean value of refractivity observed at numerous locations distributed over the globe. At each station the mean refractivity as a function of height has been fitted to two exponentials for each of four months: February, May, August and November. This data was used to compute time delay as a function of season for signals originating at various altitudes at numerous locations. Representative data is shown in Figures 4-6.

Two curves are plotted in each figure, one for the maximum corrected time delay at the given location and one for the minimum corrected time delay. In Figure 4, the corrected time delay is plotted as a function of actual aspect for the mean atmosphere above Barrow, Alaska. Figure 5 represents the same data for the mean atmosphere above Clark Field, Phillipines. Figure 6 represents the corrected time delay versus actual aspect angle based on the mean atmosphere above Puerto Montt, Chile. Each curve has been drawn for a signal which starts at an altitude of 100 km. There is very little change with altitude between 50 and 100 km, and since virtually all of the lower atmosphere lies below 100 km, those signals which originate at 100 km are indicative of the maximum effect of

the atmosphere. Note in particular, that all of these curves have essentially the same shape, that the spread between maximum delay and minimum delay is relatively small, and that there is very little quantitative difference in the delay as a function of actual aspect angle measured at any of these locations.

The locations used in Figures 4-6 were chosen because they are representative of the different climatic conditions around the world.

By way of comparison, the corrected time delay was also computed using the CRPL exponential reference atmosphere. This data is presented in Figure 7, again for an altitude of 100 km. The three curves in Figure 7 represent the minimum delay, maximum delay and an intermediate case as predicted by this model. Note, that the shape of these curves is quite similar to that for the compound bi-exponential model, although, the corrected delay at a given aspect angle is, for each case, lower than the delay predicted by the compound bi-exponential model. For example, at vertical incidence the compound bi-exponential model predicts corrected delays between about 7.5 and 8.7 nanoseconds whereas the extremes for the CRPL model are about 6.2 and 7.3 nanoseconds. However, in the case $N = 313$, $C_e = 0.1439\ (km)^{-1}$ the CRPL and compound bi-exponential models are quite close.

B. The Ionosphere

For purposes of these calculations the ionosphere has been approximated by a three part model. Below the peak electron density, it is assumed that the electron density profile is parabolic. Between the height of the peak electron density and 1,000 km, a Chapman-like function, $\exp \frac{1}{2}\left[1 - z - ze^{-h}\right]$, is assumed for the electron density profile. It is assumed that the density at 1,000 km is given by $N(1{,}000) = 8 \times 10^3 \left[1 + \cos^2 m \cos^2 (\chi/2)\right]$ where m is the magnetic dip angle and χ is the solar zenith angle, and above 1,000 km the electron density is assumed to decay exponentially to the constant value of 10^3 electrons/cc at 5,000 km. The bottom of the ionosphere is assumed to occur at 100 km and calculations of the corrected delay have been made for signals which originate between 1,000 km and 5,000 km and are received at 100 km.

In Figures 8-10 are shown curves of corrected delay versus frequency for a number of different values of peak electron density, representative of the actual ionosphere. Figure 8 displays data at vertical incidence, Figure 9 at an actual aspect angle of 30 degrees and Figure 10 at an actual aspect angle of 70 degrees. In Figure 11, the corrected time delay versus actual aspect angle is plotted for various values of peak electron density and a frequency of 1 GHz. A similar curve at a frequency of 8 GHz is shown in Figure 12. In each case $m = \chi = 0$, $H_m = 350$ km and the half-thickness of the parabolic region is 200 km.

The variation of the data with m and χ is not too great, especially for large values of peak electron density. In order to illustrate this, the data in Figures 13 and 14 was prepared in the extreme case, m = 90°. In Figure 13, corrected time delay is plotted as a function of frequency for normal incidence (an actual aspect angle of zero degrees), and in Figure 14, the corrected time delay is plotted as a function of actual aspect angle for a frequency of 4 GHz. A corresponding curve for m = 0 degrees is also indicated on Figure 14 at the peak density of 6.4×10^6 electrons/cc. In each case m = 90°, H_m = 350 km, the half-thickness of the parabolic region is 200 km and the signal originates at an altitude of 5,000 km. (The change with altitude is similar to that indicated in Figures 8-10.)

Other models for the ionosphere have also been used, although it is felt that the one used here is more representative of the actual ionosphere than any others tried. For example, a parabolic ionosphere yielded the data shown for vertical indidence in Figure 15.

C. The Composite Atmosphere

The data for the lower atmosphere and the ionosphere has been put together to predict the total propagation delay in the atmosphere. Doing so is somewhat difficult because of the many parameters involved. For example, one must specify frequency and electron density profile for the ionosphere and location and season for the lower atmosphere. However, for the purposes of predicting the total corrected time delay, the atmosphere changes very little from site to site and from month to month (see Figures 4-6). The atmosphere above Barrow, Alaska in May is reasonably representative of the typical atmospheric contribution to delay. Consequently, the calculations were made using a lower atmosphere modeled after that over Barrow, Alaska in May in conjunction with the model ionosphere described in the previous section.* The results are shown in Figures 16-18, and in each figure the corrected time delay is plotted against solid angle. (Since the propagation problem is azimuthally symmetric, the locus of all stations which receive with the same corrected delay is a circle on the earth's surface. This circle is centered about the line which joins the center of the earth and the satellite and subtends a solid angle, Ω, on the earth's surface which is plotted against the corrected time delay to obtain Figures 16-18.) For a given time delay, Δt, the corresponding solid angle obtained from Figures 16-18 identifies that portion of the earth's surface with which communications can be made at a corrected delay of less than or equal to Δt.

*In each of the cases reported here m = χ = 0, H_m = 350 km and the parabolic half-thickness is 200 km.

In Figure 16 and 17, corrected delay is plotted against solid angle for a satellite altitude of 5,000 km for various values of peak electron density. The propagation frequency in Figure 16 is 2 GHz and in Figure 17 it is 8 GHz.

In Figure 18 corrected delay is plotted against solid angle for a satellite altitude of 1,000 km, a frequency of 8 GHz and for various values of peak electron density.

Comparison of Figures 17 and 18 indicates, as one would suspect, that for a given permissible time delay and frequency, the higher of the two satellites can communicate with more of the earth's surface. This is true because the signal is more nearly vertical for the higher satellite and because the electron density is relatively small above 1,000 km.

The solid angle subtended by a circle of 3,000 miles diameter is indicated on each of the figures. Such a circle corresponds roughly to that portion of the earth's surface occupied by the continental U. S.

VI. CONCLUSIONS

The accuracy of the numerical data presented in this report is almost entirely determined by the models used for the atmosphere. In the case of the lower atmosphere the situation is reasonably well in hand. The lower atmosphere has been studied extensively, over long periods of time and most of its irregularities are restricted to a relatively small, near the surface, region. On an average basis, the compound bi-exponential model represents the local refractivity profile to within a few percent over most of the globe. However, the model for the ionosphere is much less reliable. The dynamics of the ionosphere are quite complex and only relatively recently have the upper extremities of the ionosphere been available for study. Furthermore, the ionosphere encompasses a much more vast region of space than does the lower atmosphere. A realistic, quantitative, evaluation of the model used herein for the ionosphere is difficult; however, it was based on relatively recent observations of the density profiles.

Of course, the models are only intended as first order representations of the atmosphere and are not intended to describe inhomogeneities and time variations in the media. For the most part these phenomena are second order effects; however, a few such phenomena should command attention. For example, the effect of rain and fog on propagation delay as opposed to attentuation, and the effect of time varying, small scale inhomogeneities on the timing signal. When propagation occurs over large distances, one should also be concerned with the effect of large scale inhomogeneities on the timing signal, as for example, weather fronts, and the changes in electron density which accompany the changing, local, solar zenith angle.

It also should be noted that in this investigation attention has been focused on a frequency range from about 1 to 15 GHz. This is the "window" between the absorption peak of water vapor at about 22.5 GHz and the realm in which the ionosphere must be treated as an anisotropic (eventually opaque) medium. At the high frequency end of this spectrum some attention should be devoted to attenuation due to scattering from rain, fog, etc., and at the low end of this spectrum inhomogeneities in the ionosphere may require attention. The possible use of higher frequencies, perhaps optical frequencies, in a one-way timing system may warrant some future extension of this frequency spectrum.

In total, this report has aimed at summarizing the nature of the atmosphere, at outlining the techniques used to calculate propagation time delay through the atmosphere, and at making a reliable, but first order, calculation of the effect of the atmosphere on the propagation of timing signals at frequencies between about 1 GHz and 15 GHz.

VII. ACKNOWLEDGMENTS

This work was started during the NASA Summer Faculty Fellowship program, 1970, at the Goddard Space Flight Center. Special thanks are due Mr. Andrew Chi who made the completion of this work possible and Mr. John Lavery who assisted most competently with the numerical work.

BIBLIOGRAPHY

1. Univ. of Michigan Summer Conferences, on High Altitude Sciences, 1964.

2. Debye, P., Polar Molecules, Dover, New York, N. Y., 1957.

3. Bean, B. R., "The Radio Refractive Index of Air," Proc. IRE, March 1962, pg. 260-273.

4. Smith, E. K., and Weintraub, S., "The Constants in the Equation for Atmospheric Refractive Index at Radio Frequencies," Proc. IRE, August 1963, pg. 1035-1037.

5. U. S. Standard Atmosphere, 1962; Sup. of Doc., U. S. Gov. Printing Office, Wash. 25, D. C.

6. Bean, B. R., "Models of the Atmospheric Radio Refractive Index," Proc. IRE May 1959, pg. 740-757.

7. Bean, B. R., "Tropospheric Refraction," Advances in Radio Research, Saxton, J. A., Ed., Academic Press, Vol. 1, 1964, pg. 53-120.

8. Bean, B. R. and Dutton, E. J., Radio Meteorology, NBS Mono. #92, March 1966.

9. The Rocket Panel, "Pressures, Densities and Temperatures in the Upper Atmosphere," Phy. Rev., Vol. 88, pg. 1027-1032.

10. Misme, P., "Models of the Atmospheric Radio Refractive Index", Proc. IRE, Vol. 48, pg. 1498-1499.

11. Bean, B. R. and Thayer, G. D., Proc. IRE, Vol. 48, pg. 1499-1501.

12. Bean, B. R., Cahoon, B. A., Samson, C. A., Thayer, G. D., "A World Atlas of Atmospheric Radio Refractivity," ESSA Mono. #1, 1966.

13. Ratcliffe, J. A., Physics of the Upper Ionosphere, Academic Press, 1960.

14. VanZandt, T. E. and Knecht, R. W., "The Structure and Physics of the Upper Atmosphere," Space Physics, Le Galley and Rosen, Ed., John Wiley and Sons, New York, N. Y., 1964.

15. Ionospheres and Radio Physics 1958-1964, NASA SP-95, 1966.

16. Chapman, S. J., "The Absorption and Dissociative or Ionizing Effect of Monochromatic Radiation in an Atmosphere on a Rotating Earth," Proc. Phys. Soc., London, Vol. 43, 1931, pg. 26-45.

17. Chapman, S. J., "The Absorption and Dissociative or Ionizing Effect of Monochromatic Radiation in an Atmosphere on a Rotating Earth. Part II Grazing Incidence", Proc. Phys. Soc. London, Vol. 43, 1931, pg. 483-501.

18. Davies, K., Ionospheric Radio Propagation, NBS Mono. #80, April 1965.

19. Martyn, D. F., "The normal F-Region in the Ionosphere," Proc. IRE, Feb. 1959, pg. 147-155.

20. Hayden, G. W. and Lucas, D. L., "Predicting Ionospheric Electron Density Profiles," Radio Science, Vol. 3, #1, January, 1968, pg. 111-119.

21. Kelso, J. M., Radio Ray Propagation in the Ionosphere, McGraw-Hill, New York, New York, 1964.

22. Lawrence, R. S., and Little, C. G., "A Survey of Ionospheric Effects Upon Earth-Space Radio Propagation," Proc. IEEE, Jan. 1964, pg. 4-27.

23. Born, M. and Wolf, E., Principles of Optics, MacMillan, New York, 1964.

24. Bean, B. R., "Attenuation of Radio Waves in the Troposphere," Advances in Radio Science, Saxton, J. A., Ed., Academic Press, Vol. 1, 1964, pg. 121-156.

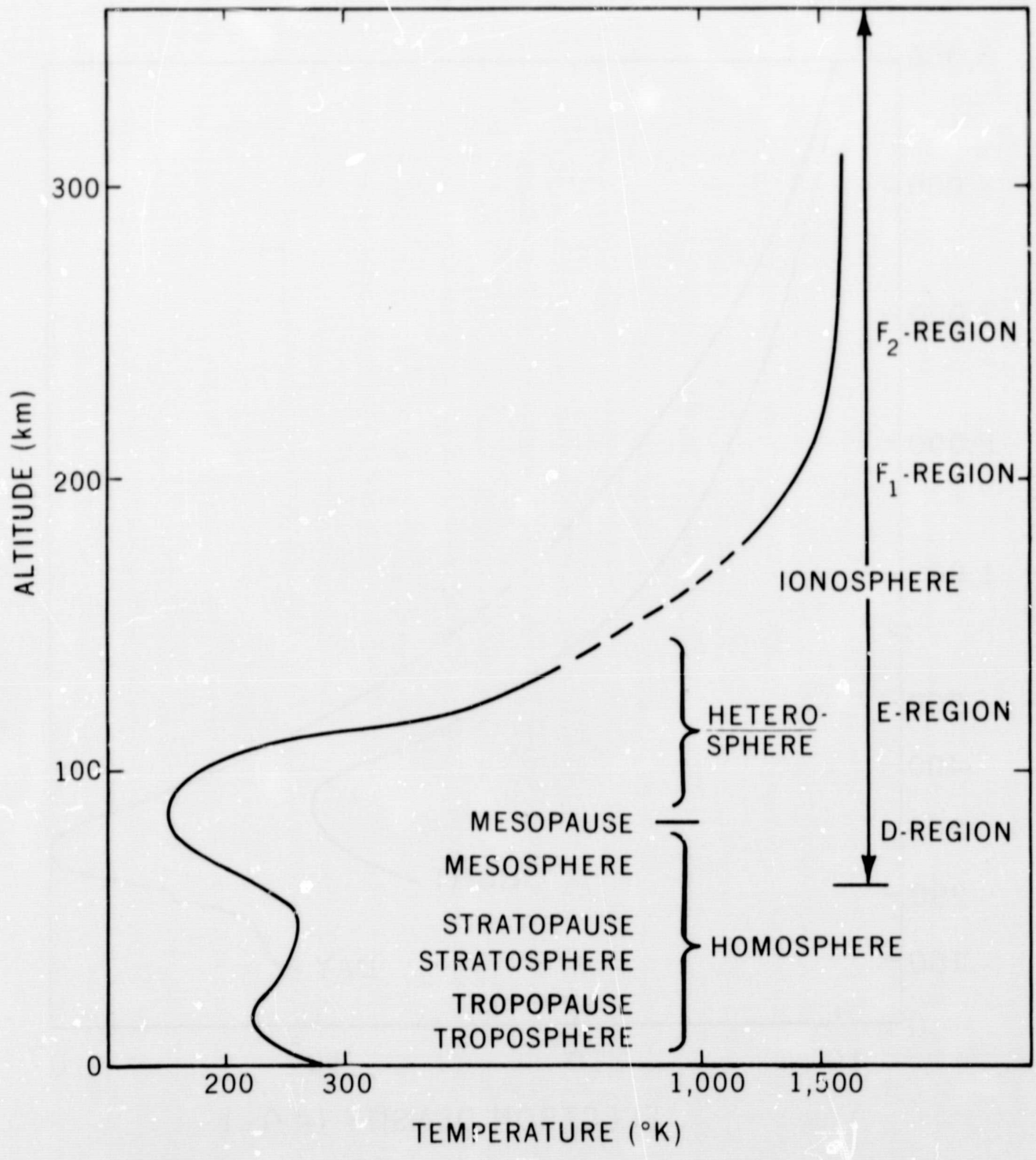

Figure 1. The Regions of the Atmosphere (Temperature Profile)

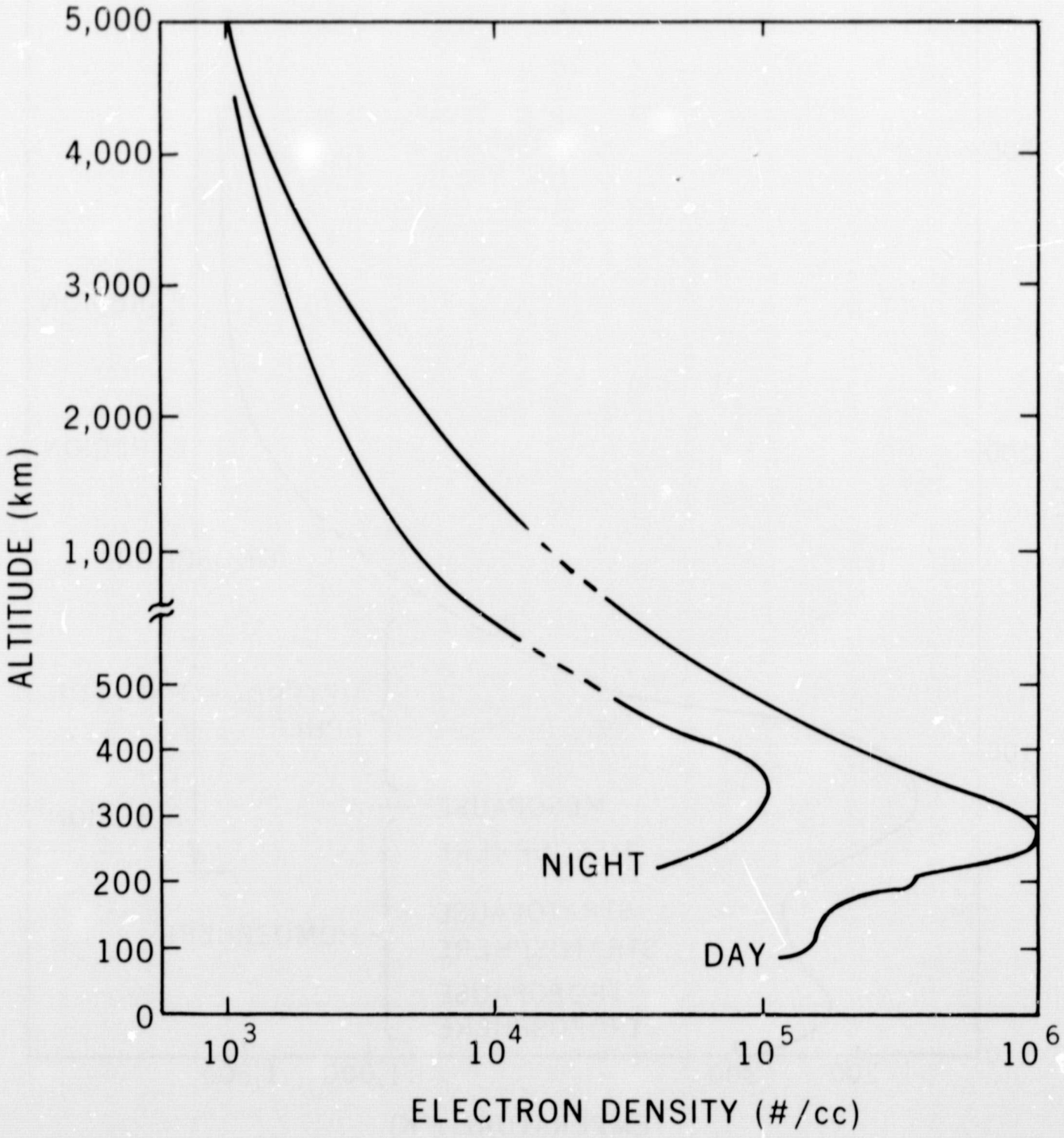

Figure 2. Example Electron Density Profiles

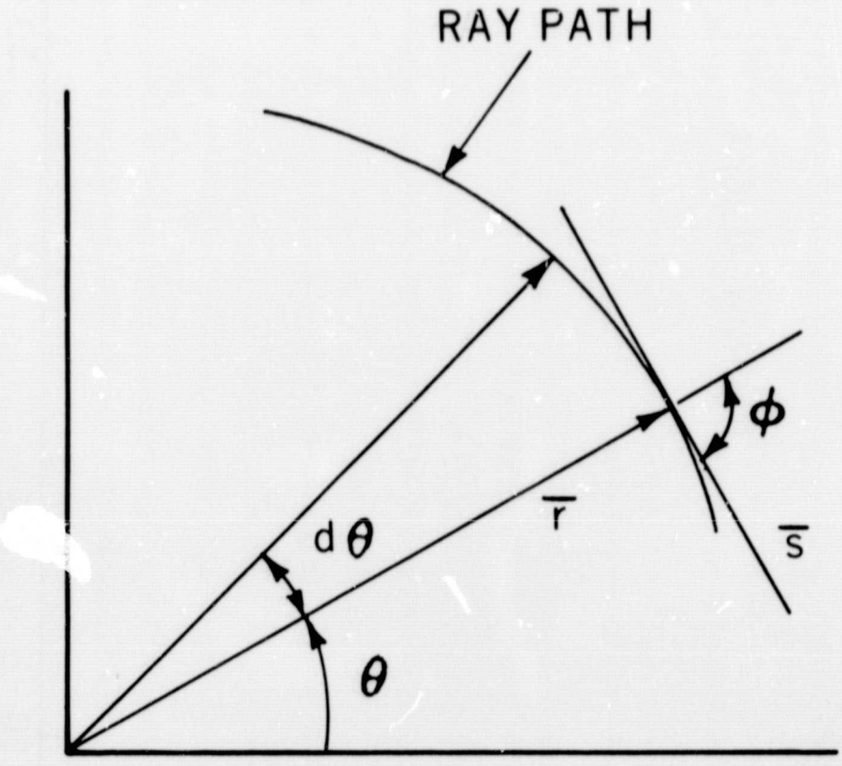

Figure 3. The Geometry for Ray Computation

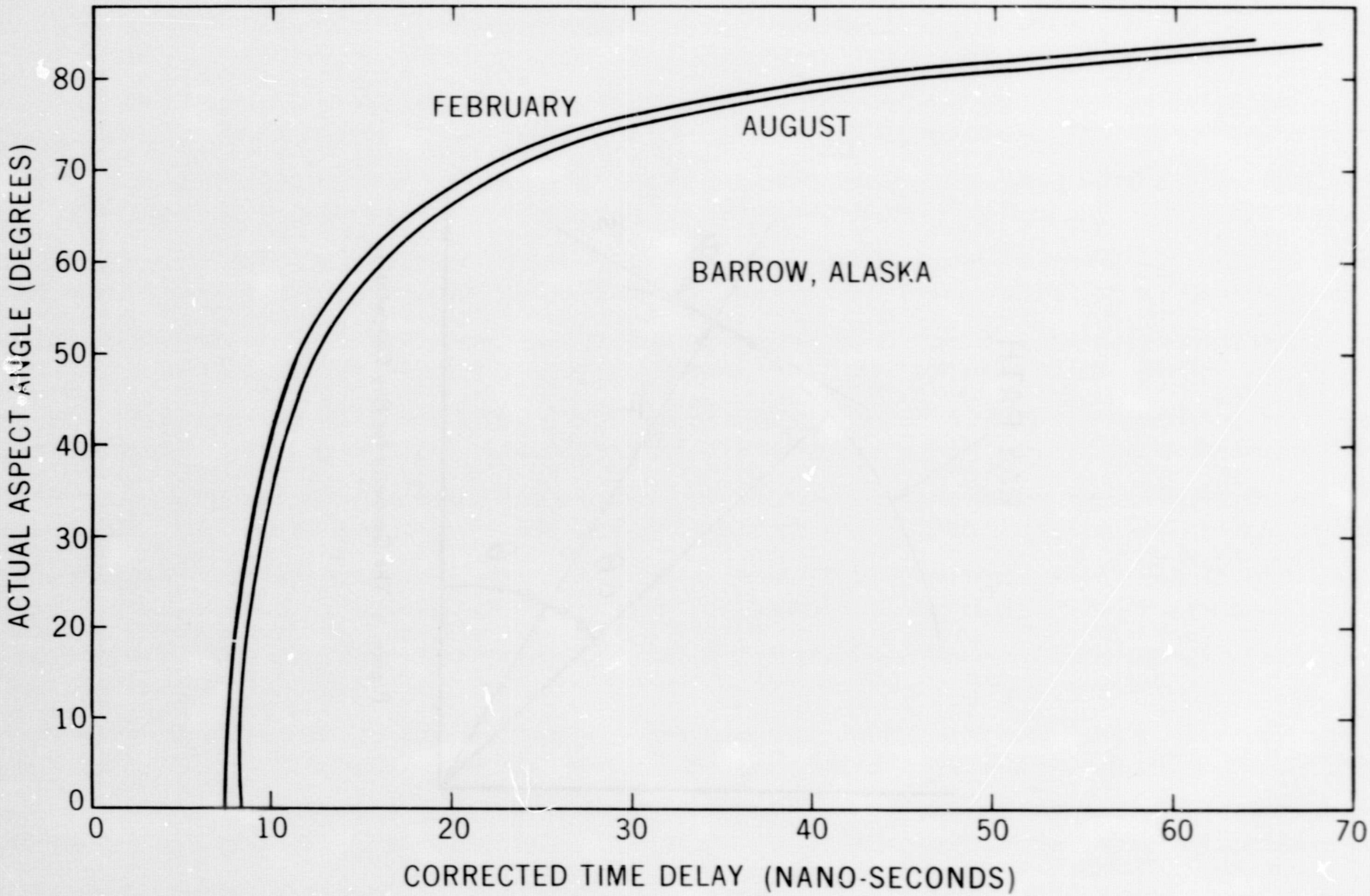

Figure 4. Corrected Time Delay in the Lower Atmosphere vs Actual Aspect Angle

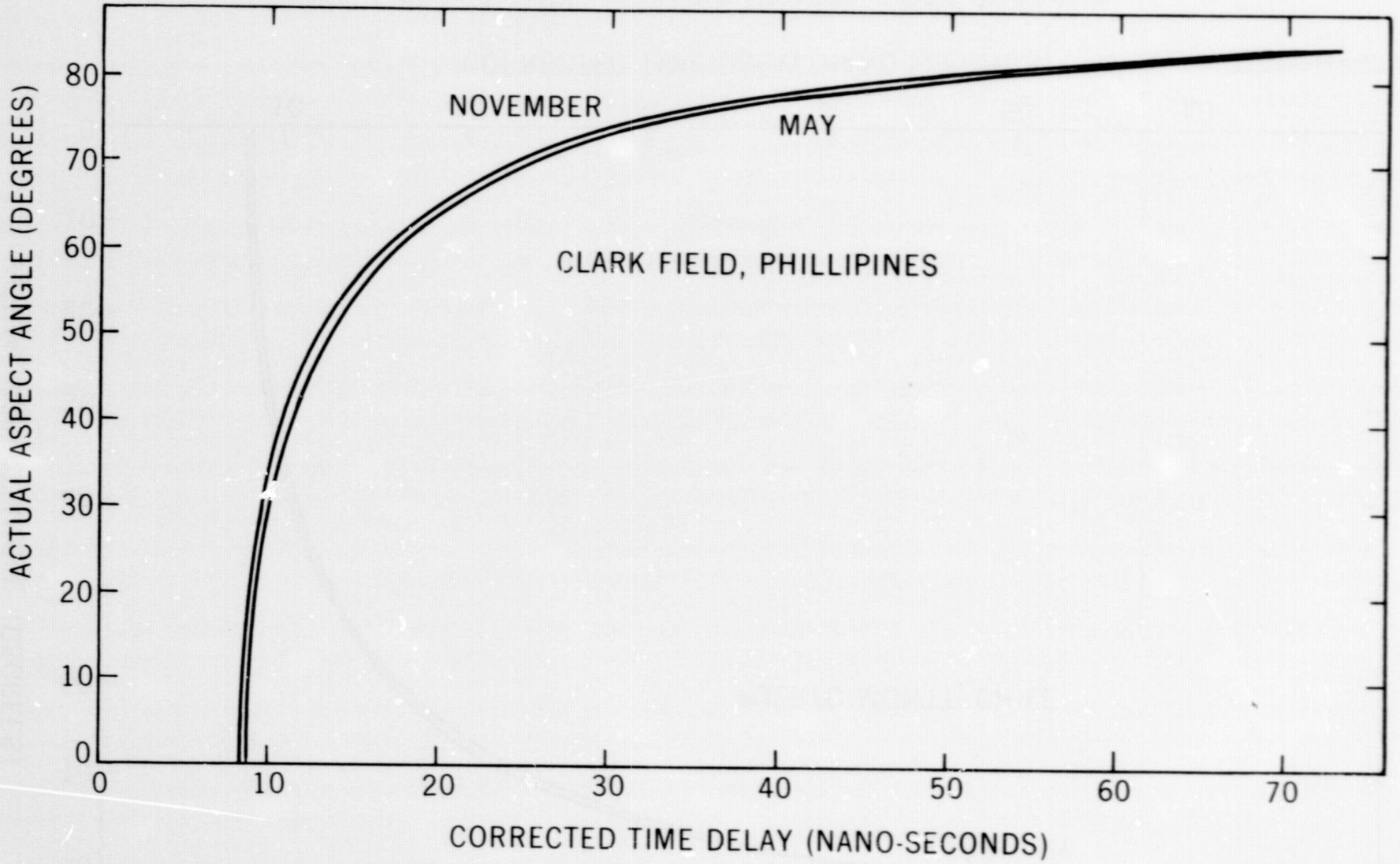

Figure 5. Corrected Time Delay in the Lower Atmosphere vs Actual Aspect Angle

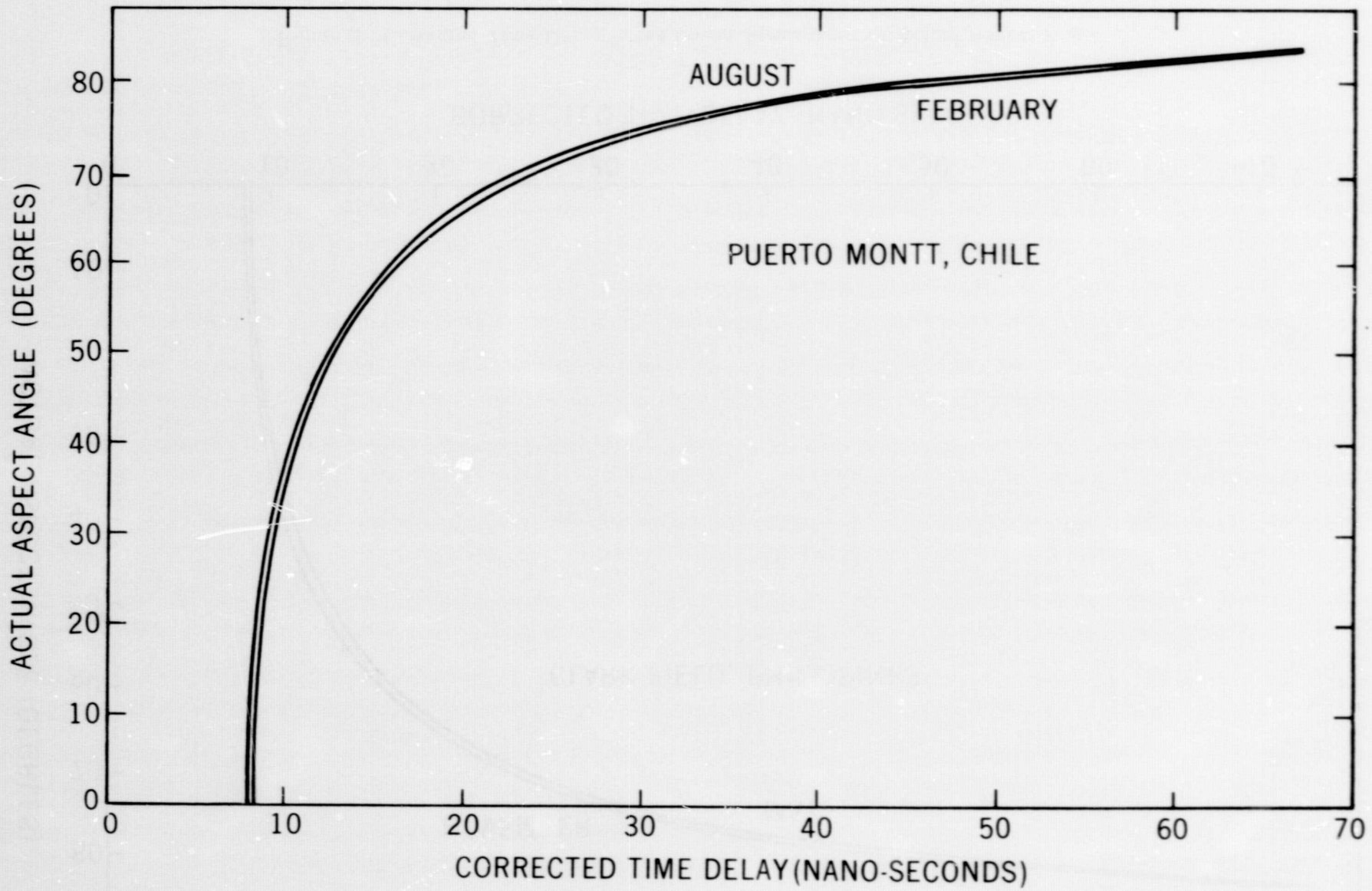

Figure 6. Corrected Time Delay in the Lower Atmosphere vs Actual Aspect Angle

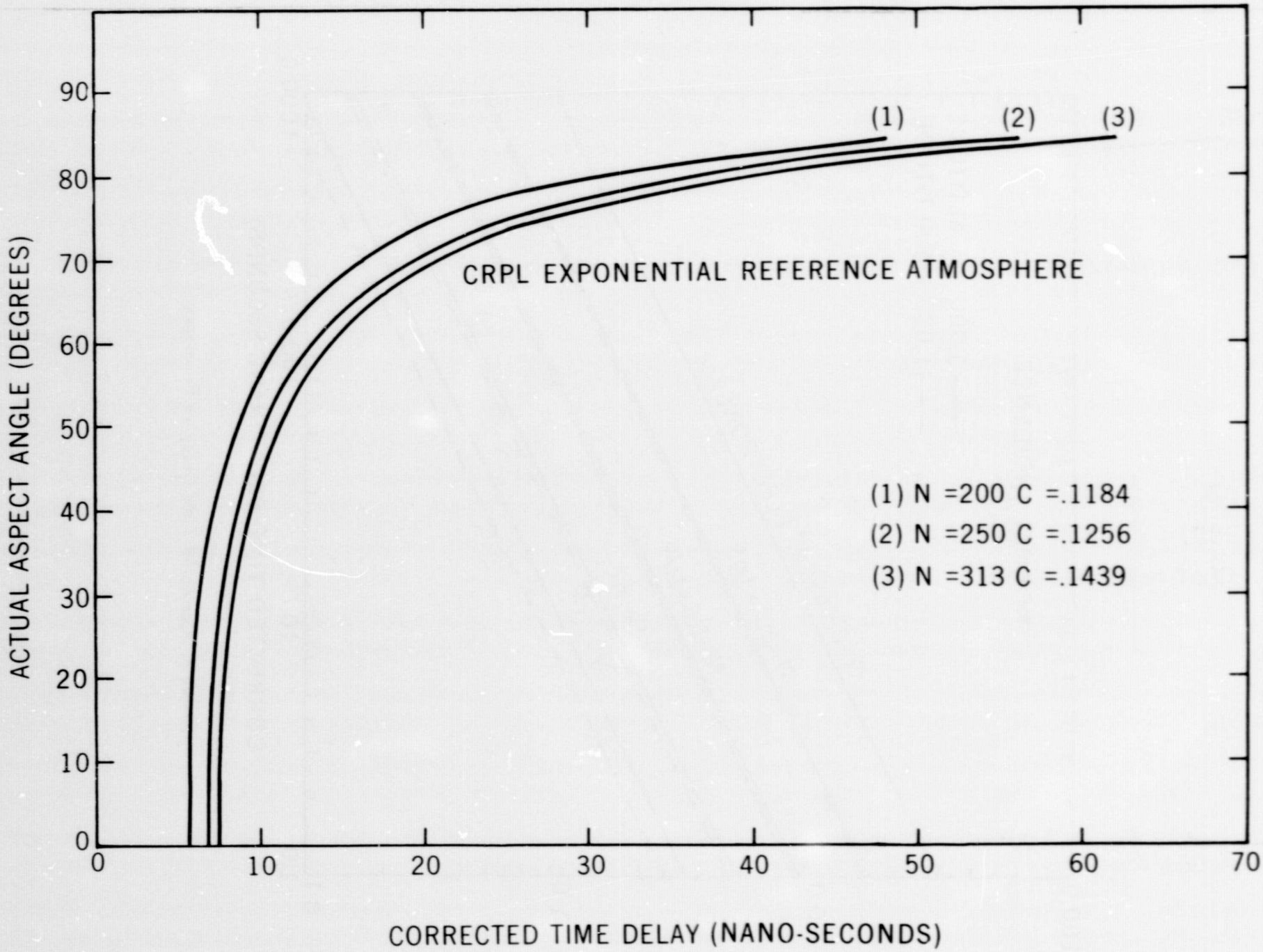

Figure 7. Corrected Time Delay in the Lower Atmosphere vs Actual Aspect Angle

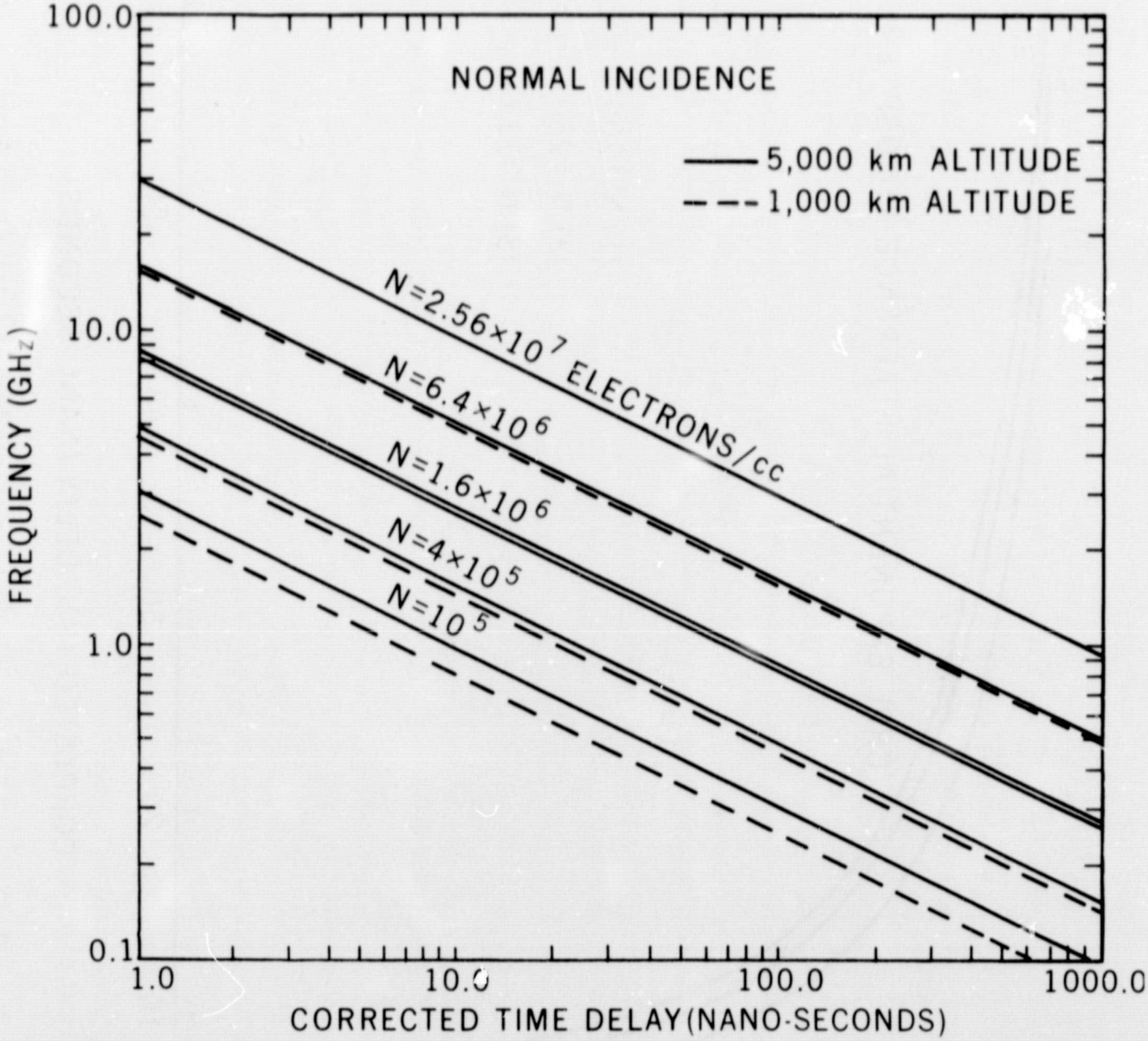

Figure 8. Corrected Time Delay vs Frequency

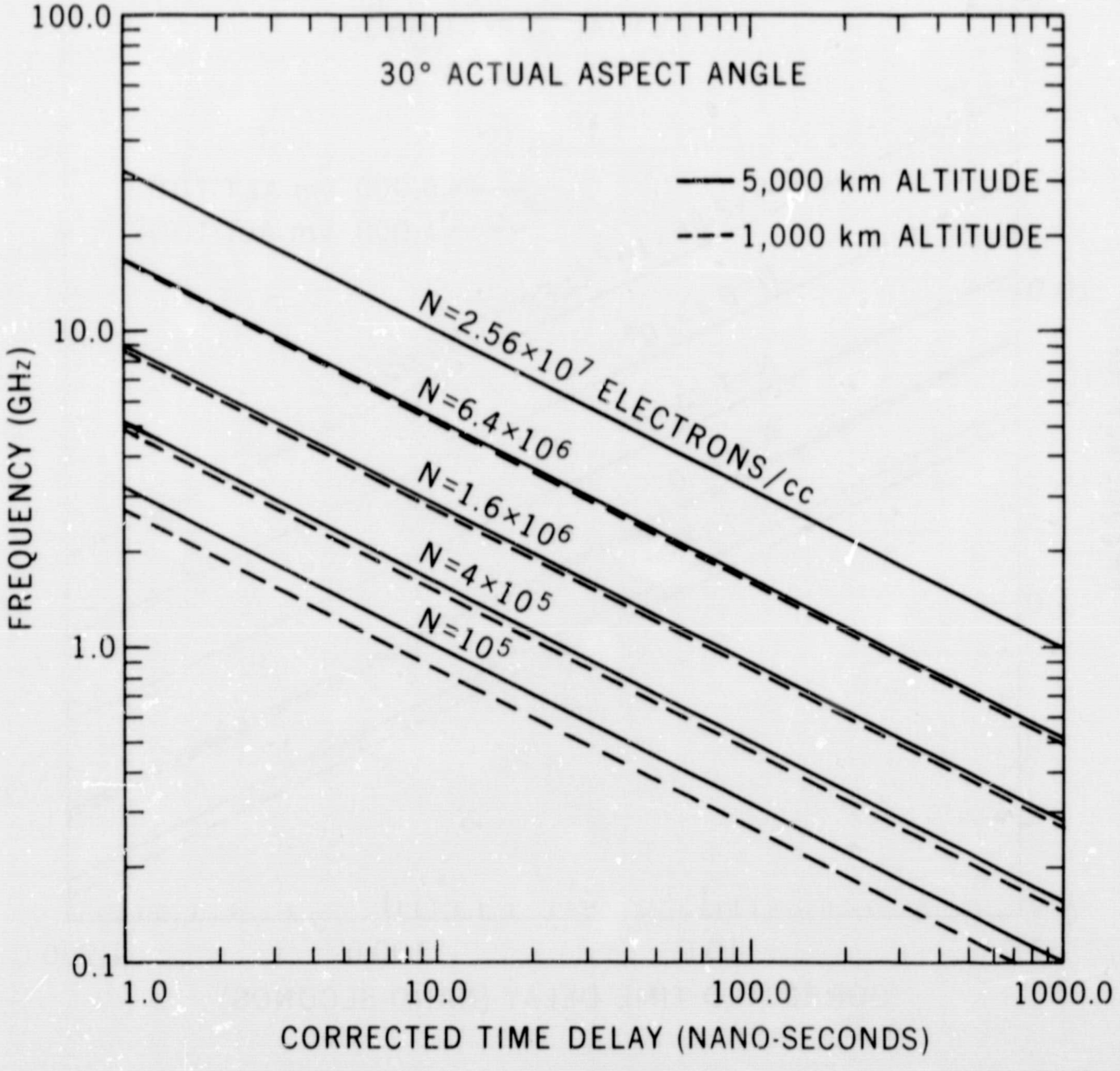

Figure 9. Corrected Time Delay vs Frequency

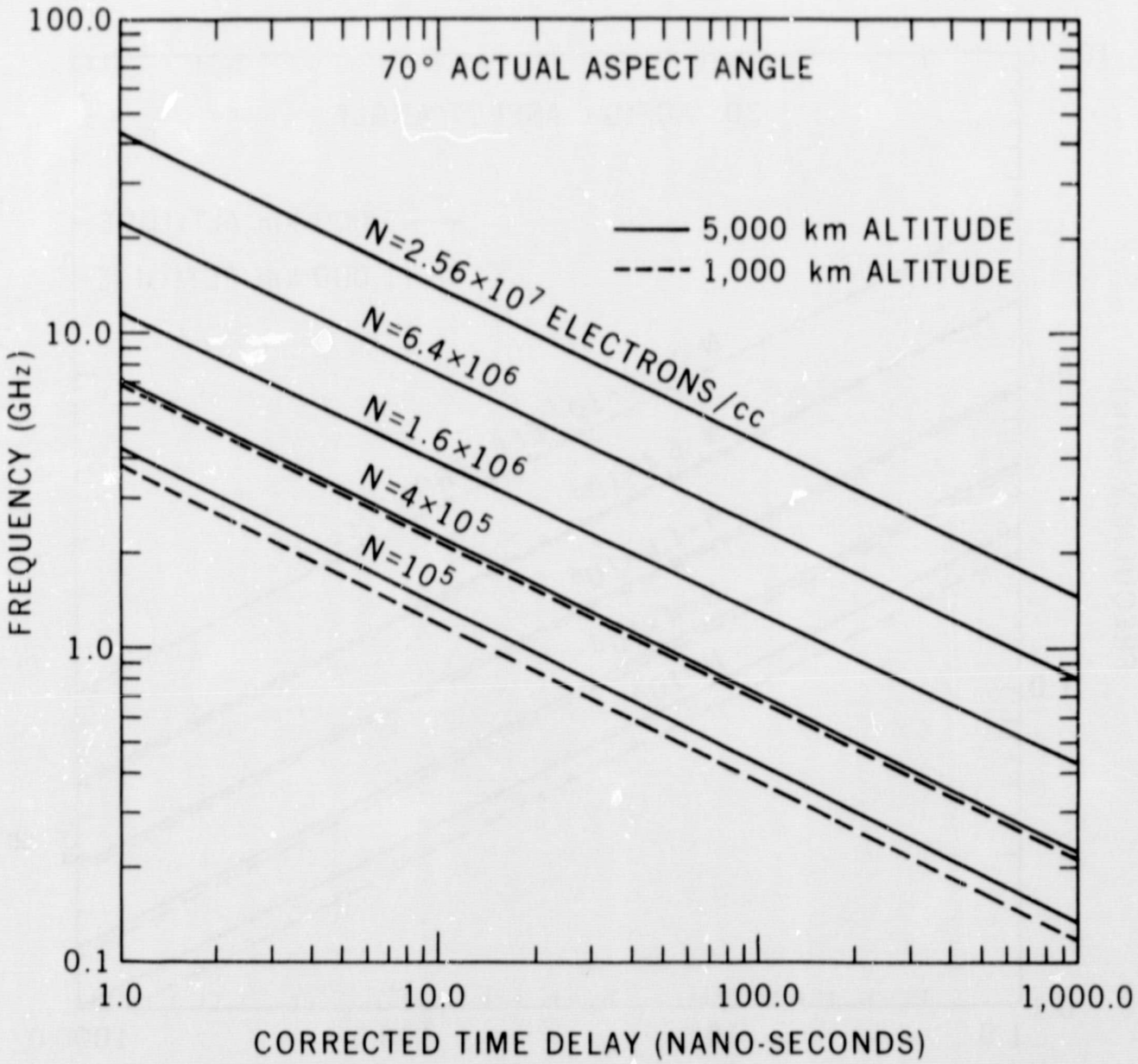

Figure 10. Corrected Time Delay vs Frequency

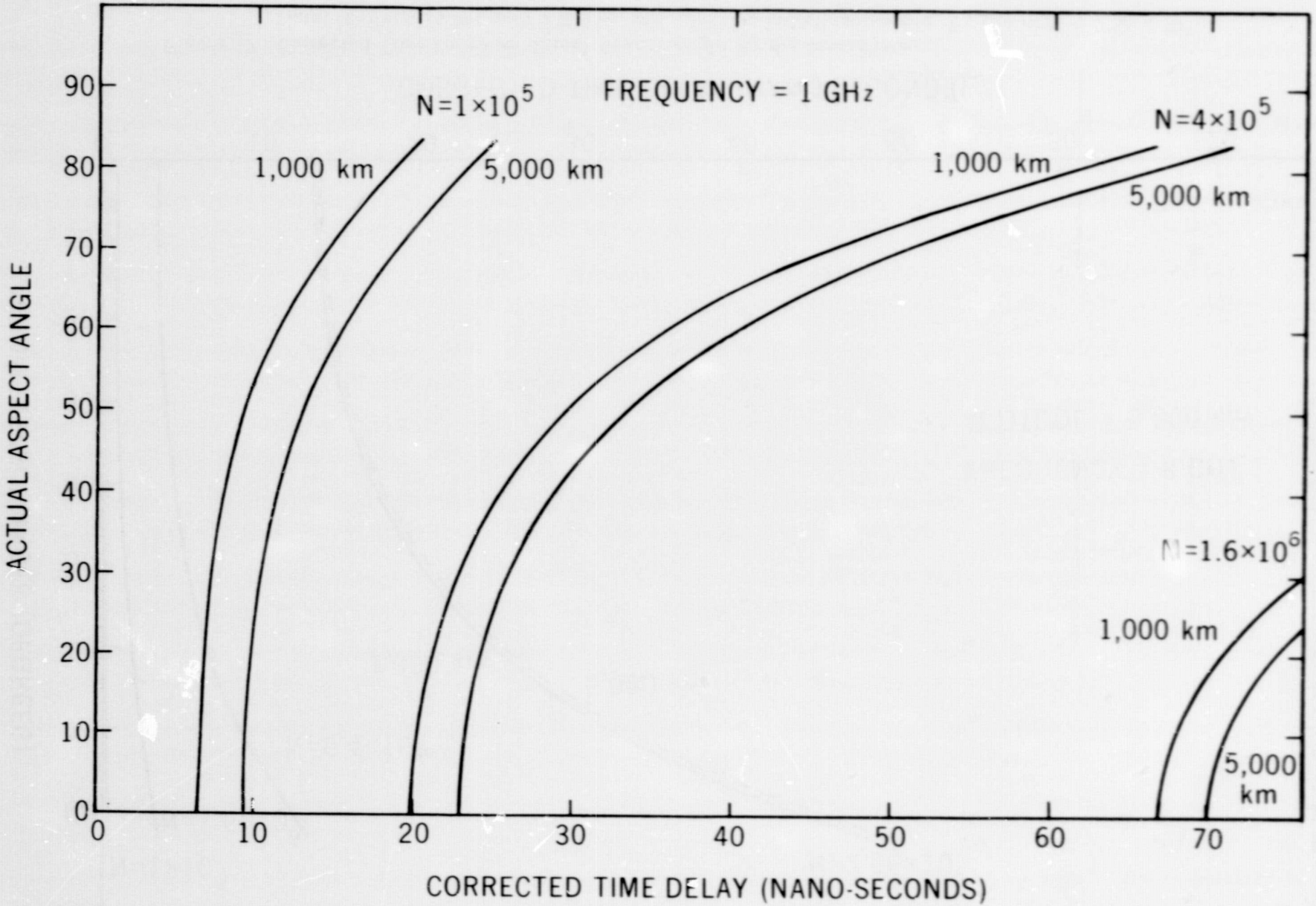

Figure 11. Corrected Time Delay vs Actual Aspect Angle

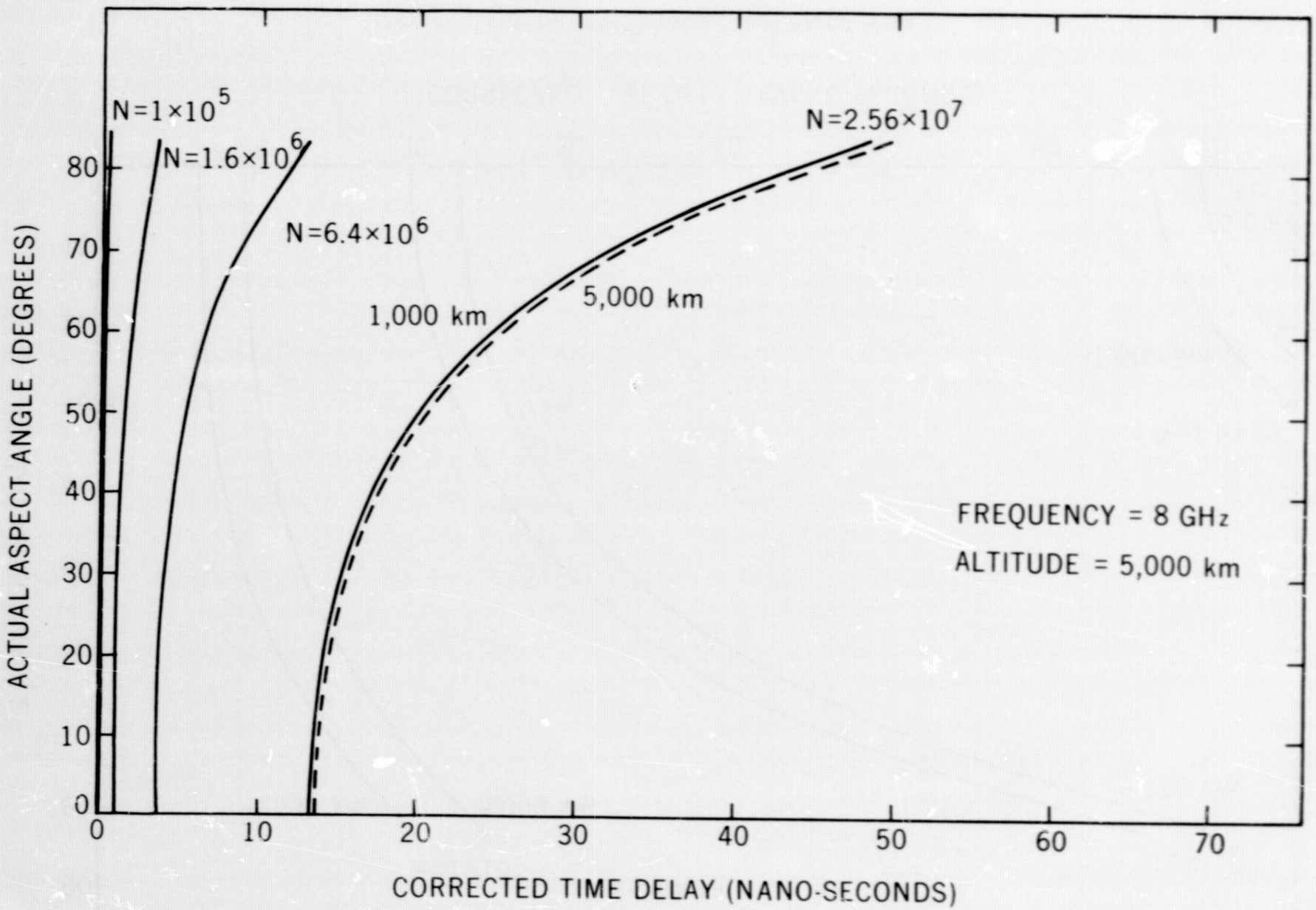

Figure 12. Corrected Time Delay vs Actual Aspect Angle for the Ionosphere.
Note: Difference between 5,000 km and 1,000 km Indistinguishable, Except at N = 2.56×10^7.

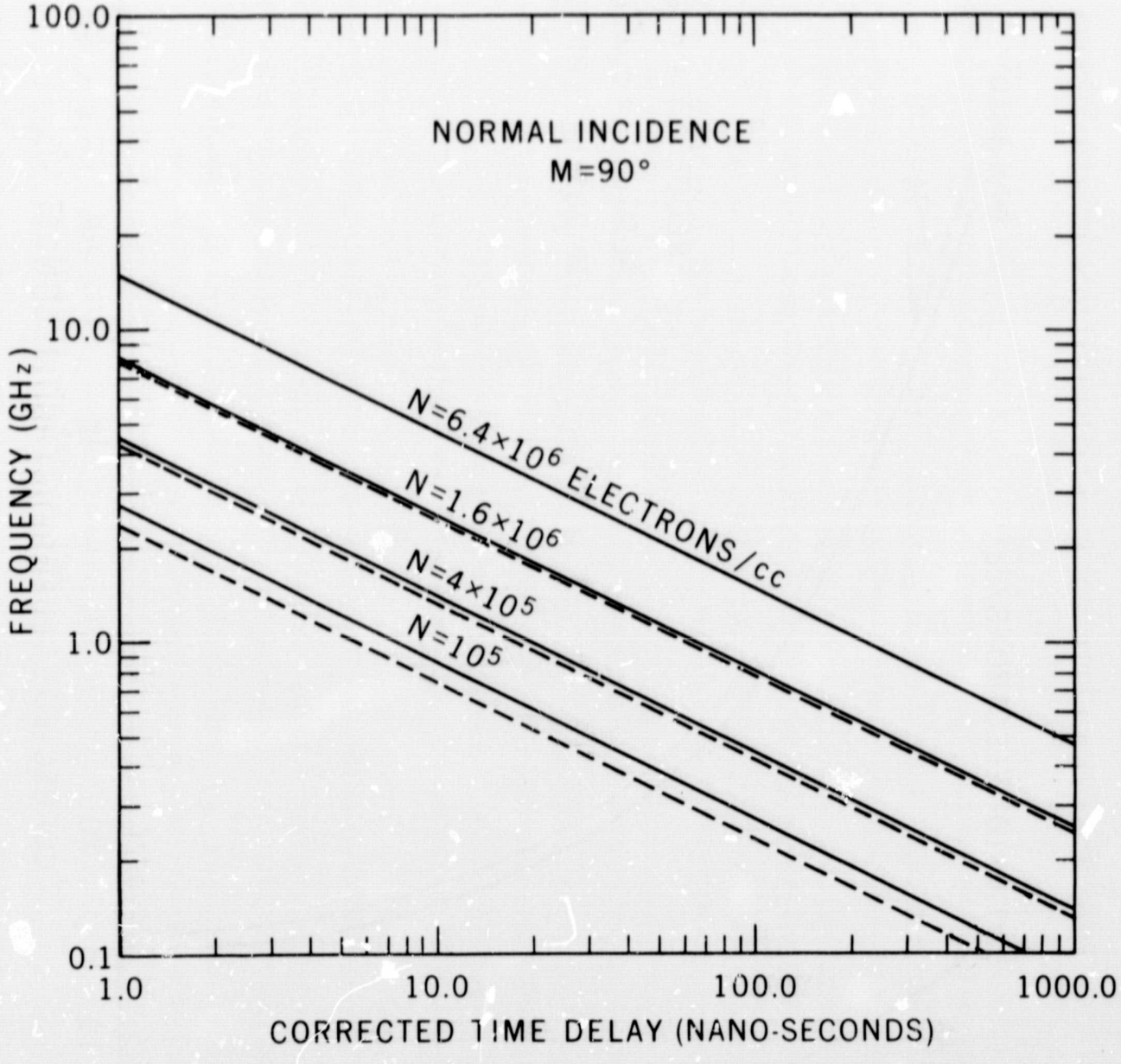

Figure 13. Corrected Time Delay vs Frequency

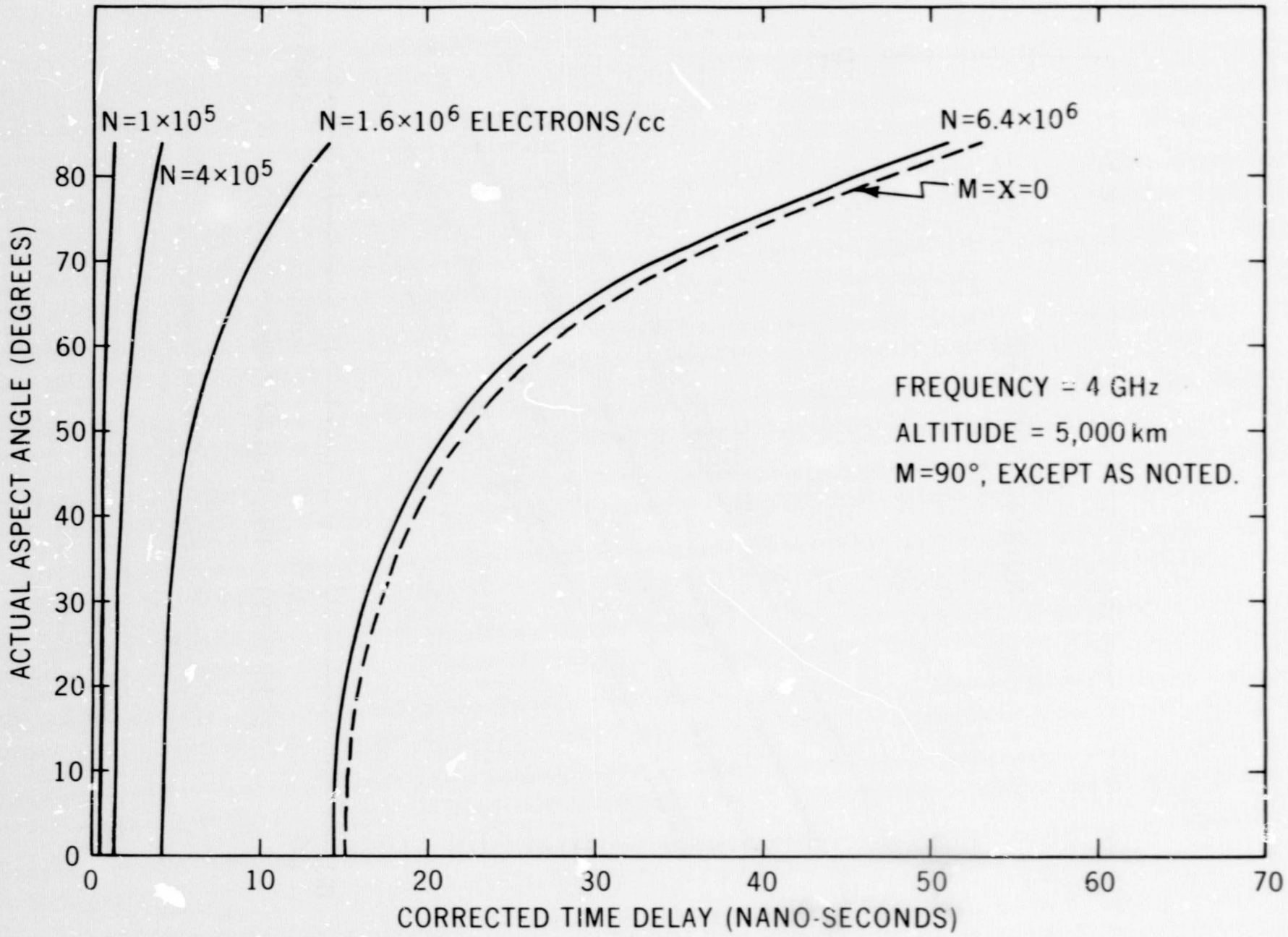

Figure 14. Corrected Time Delay vs Actual Aspect Angle

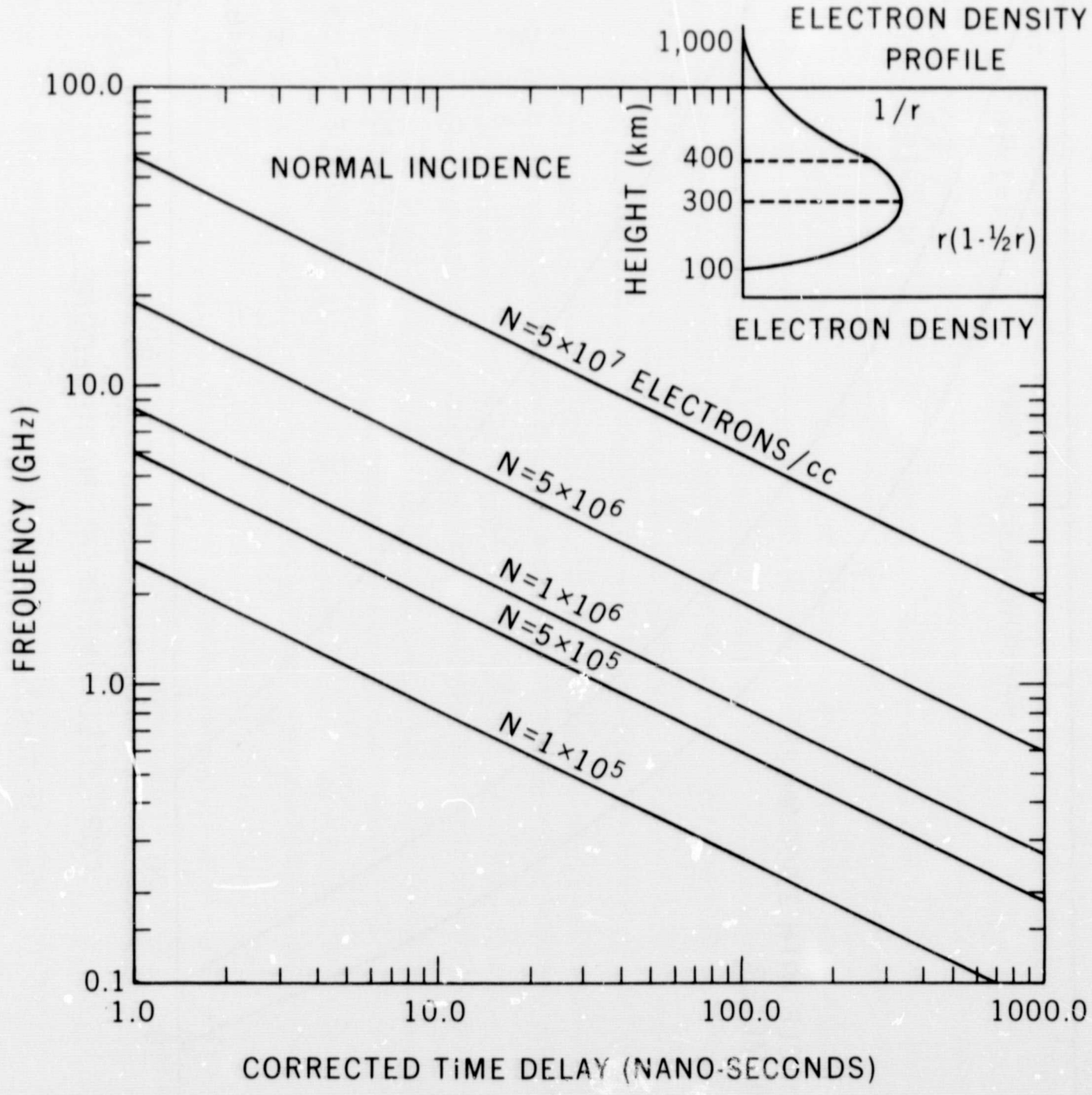

Figure 15. Corrected Time Delay vs Frequency for a Parabolic Ionosphere

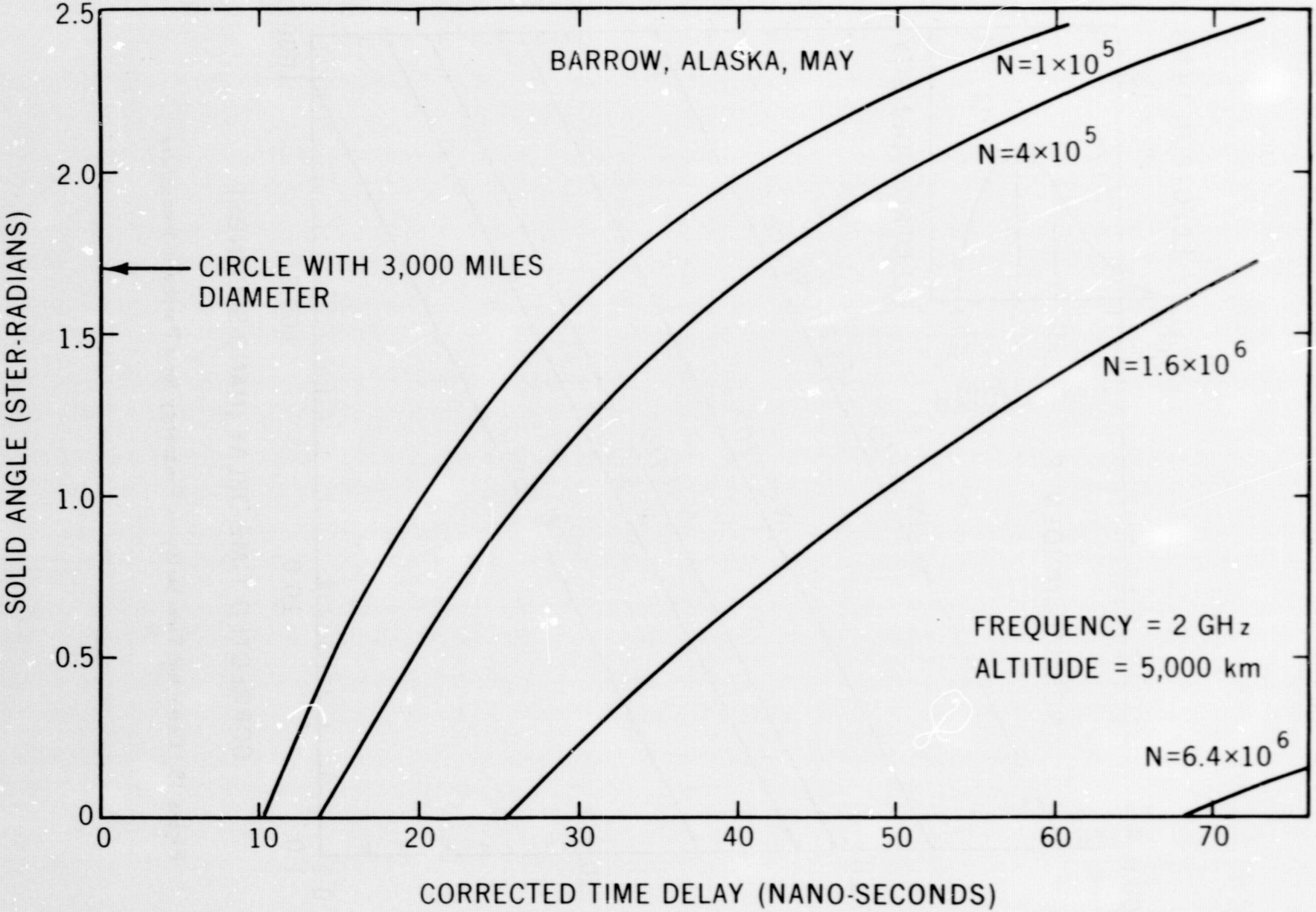

Figure 16. Total Atmospheric Corrected Time Delay

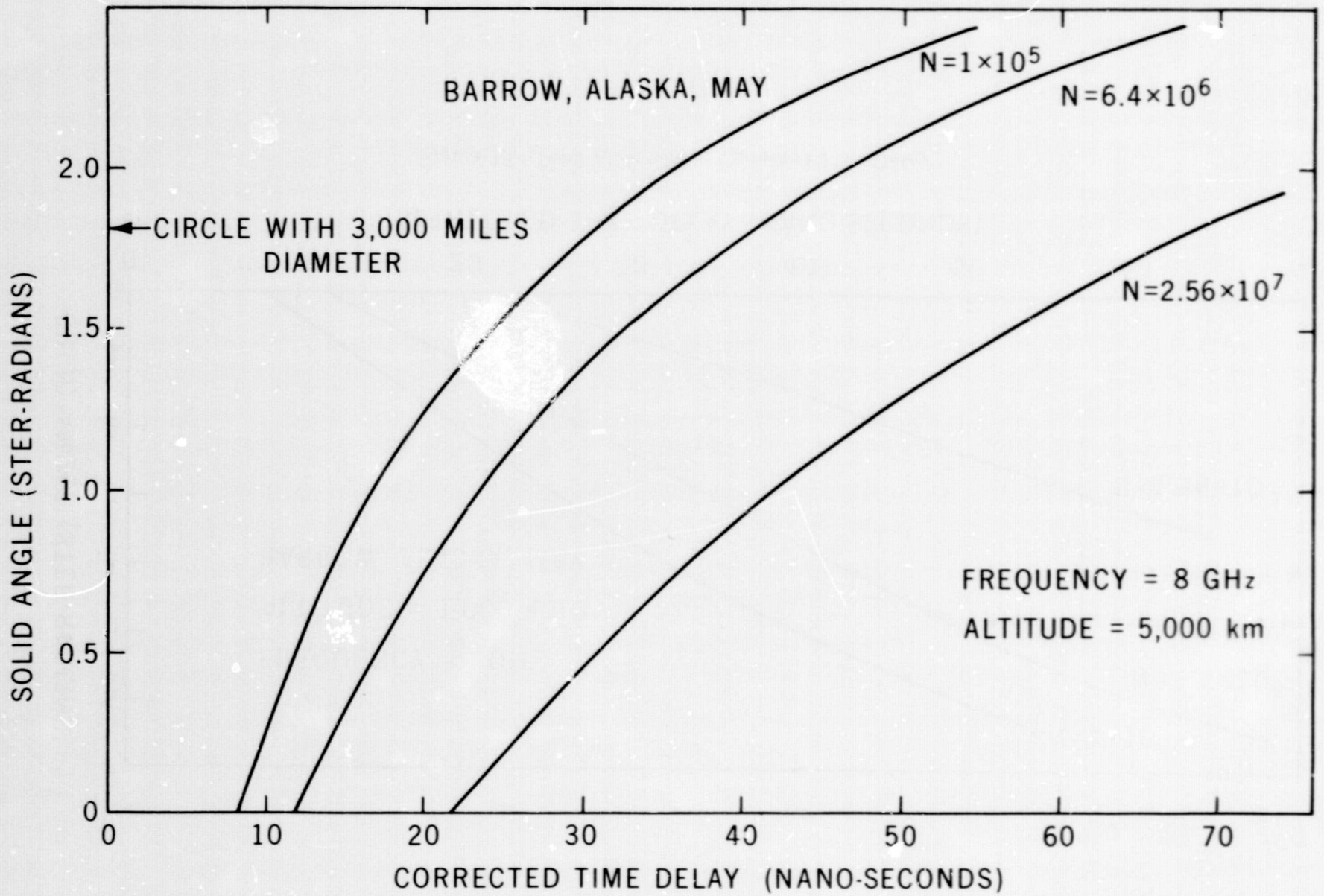

Figure 17. Total Atmospheric Corrected Time Delay

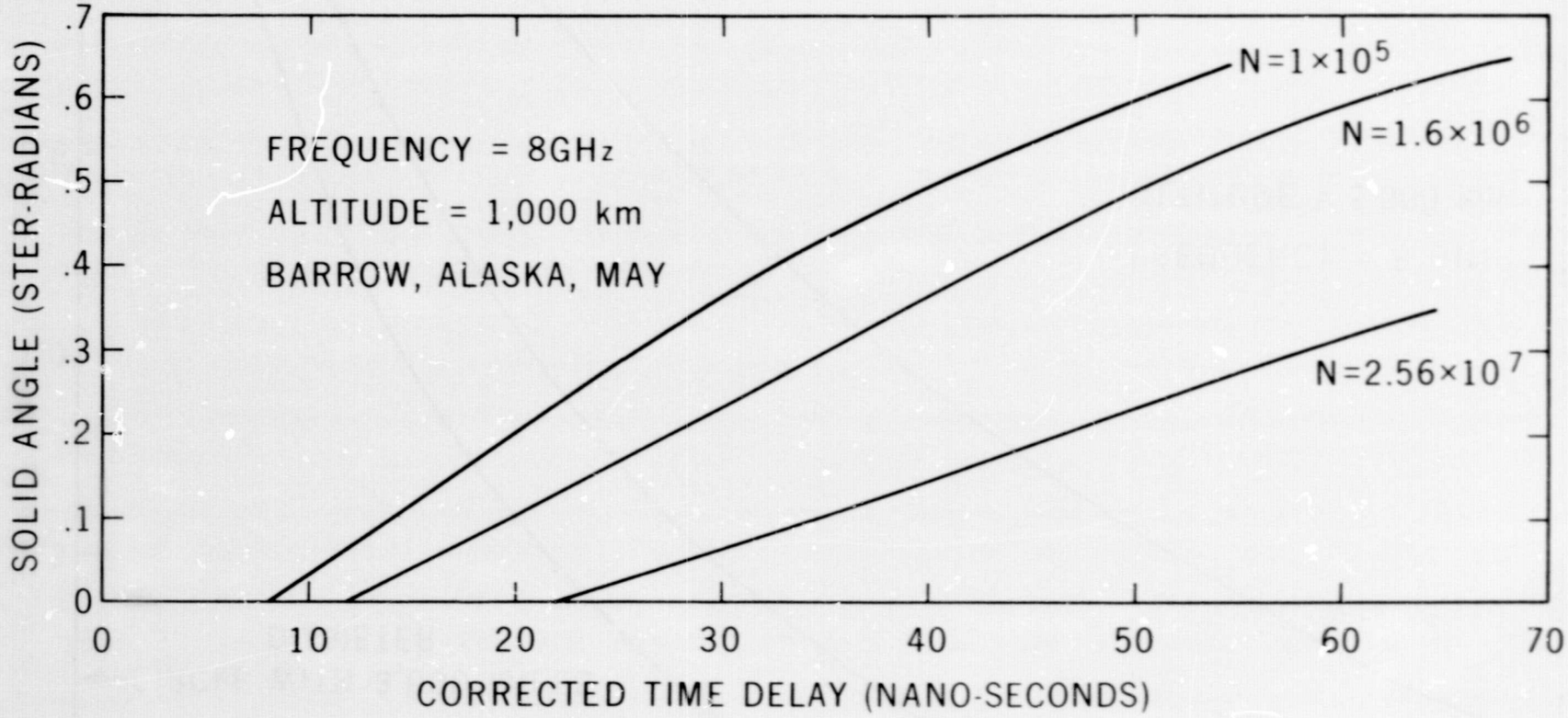

Figure 18. Total Atmospheric Corrected Time Delay